Mechano-chemical interface processes with application to rock weathering

Anja Røyne

Thesis submitted for the degree of Philosophia Doctor
Department of Physics, University of Oslo, Norway

January 2011

Series of dissertations submitted to the
Faculty of Mathematics and Natural Sciences, University of Oslo
No. 1073

ISSN 1501-7710

Cover: Inger Sandved Anfinsen.
Printed in Norway: AIT Oslo AS.

Produced in co-operation with Unipub.
The thesis is produced by Unipub merely in connection with the
thesis defence. Kindly direct all inquiries regarding the thesis to the copyright
holder or the unit which grants the doctorate.

til Tord og Synne

Preface

The subject of this thesis is coupled mechanical and chemical processes that take place at interfaces in rocks during weathering, and which have an effect on the chemical and physical transformation of the rock. It is put in the context of rock weathering, but is also relevant to other research areas such as material science.

The research is at the cross-section between physics, geology and physical chemistry. The methods used include field work, theory and laboratory experiments. Coming from primarily an experimental physics background, I feel very lucky to have had the opportunity to expand my knowledge in these different directions.

In geological studies, we are faced with the end result of millions of years of coupled processes which have taken place under largely unknown conditions. Laboratory studies offer a chance to study isolated processes under controlled conditions. Theoretical studies allow us to explore the consequences of what we know, and of what we think we know, in beautiful, simple geometries with well defined boundary conditions. I think that in order to fully understand the how the Earth works, it is necessary to combine these three approaches. This thesis takes one tiny step towards that goal.

I have had three excellent supervisors who have helped me out along the way. I'd like to thank Bjørn Jamtveit particularly for welcoming me to PGP with open arms, and for taking me on field trips to Svalbard and South Africa. Bjørn has also spent countless hours with me at the microscope and the microprobe, trying to make sense of these extrordinarily difficult and complicated rocks and to do something about my ignorance on elementary geology and chemistry.

Anders Malthe-Sørenssen has been my theoretical support, and since he knows just about everything, it always pays off to stop by his office for help and advice.

My principal supervisor has been Dag Kristian Dysthe. He has also been a great co-worker in my laboratory studies. Experimental work is something which has to be learned by doing, and I have been fortunate to learn from

Dag's wealth of experience, and to benefit from his contagious enthusiasm and creativity.

There are some other people without whom my lab activities would have been much more troublesome. Olav Gundersen has very patiently helped me with large and small practical issues and has had to deal with my frequent frustrations over things not working. Big thanks also go to Finn, Steinar, Øyvind, Helge and the other guys at the workshop who have made my clumsy constructions become working equipment. Lab work would also have been much more frustrating and less fun without the good company and enormous amount of help I've received from my fellow experimentalists, including Jan Bisschop, Anders Nermoen, Christophe Raufaste, Matthieu Angeli, Delphine Croizé, Julien Scheibert, Olivier Galland and Simon De Villiers.

Then there are some people at PGP who know "everything" and are always willing to take the time to share their wisdom. I would particularly like to thank Paul Meakin, Francois Renard, Ray Fletcher, Jens Feder and Håkon Austrheim for everything they have taught me.

Thanks to past and present office mates - Hans, Marta, Andreas and Harry - for the good compay. Jan Ludvig, Ingrid, Jaqueline, Maya, Luiza, Nina, Filip, Kirsten, Marcin&Marcin, Espen, Karen, Karin, Trine-Lise and all you other PGPans, you are a fantastic bunch of talented and friendly people.

During the course of my PhD studies a number of things have happened in my life. I have lost two people dear to me, my mother and my grandmother, but I also got married and had two wonderful children. Although these events have sometimes severely distracted me from my work, I have never had anything but support from my colleagues and supervisors, and to that I am grateful.

I would also like to acknowledge the support from friends and family outside of work. You're such great people, and just the fact that you're reading this means you are actually making an effort at understanding this project which I can never seem to explain in a very clear manner.

Asbjørn, my love, my life would have been much poorer without you. Thanks for doing all of the Christmas preparations while I was finishing my thesis.

Tord and Synne, I dedicate the thesis to you. When you're old enough to read this, I want you to know that the best part of every day during this time was coming home to see you.

Oslo, January 2011
Anja Røyne

Contents

Chapter 1

Introduction

Most rocks are formed at pressures and temperatures exceeding those at the Earth's surface (Figure 1.1). When such rocks are brought to the surface through uplifting process, they become thermodynamically unstable with respect to the prevailing conditions. Weathering refers to the in situ breakdown and transformation of rocks to equilibrate with the conditions at or near the surface of the Earth. The principle agent of rock weathering is water, and the driving force for weathering is solar energy.

Weathering is an important part of the rock cycle together with erosion, which are the processes by which rock debris is transported from the weathering site by agents such as ice, water and wind. When weathering products are transported by erosion and subsequently deposited on riverbeds, lakes and oceans, they are called sediment, which may transform to sedimentary rock through burial and cementation.

Even slight variations in rock properties and climatic conditions may lead to significant differences in weathering rates. This leads to the formation of topological features, both on small and large scales, and thereby directly affects the shape of the world we live in.

When organic matter becomes part of the sediment and is transformed into sedimentary rock, nutrients and building-blocks which are essential for life becomes locked in the rock cycle. Weathering is the process by which these nutrients are released back into the biosphere, and it is therefore critical for the existence of life on the planet [1]. Weathering also affects the long term global climate because precipitation of carbonates during weathering binds CO_2 from the atmosphere [1, 2]. On shorter timescales, weathering has a direct effect on the human society through its destructive effect on concrete and building stones [3].

Weathering also produces some stunningly beautiful and intriguing patterns that we observe around us (e.g. Figure 1.2c-e). Patterns trigger our

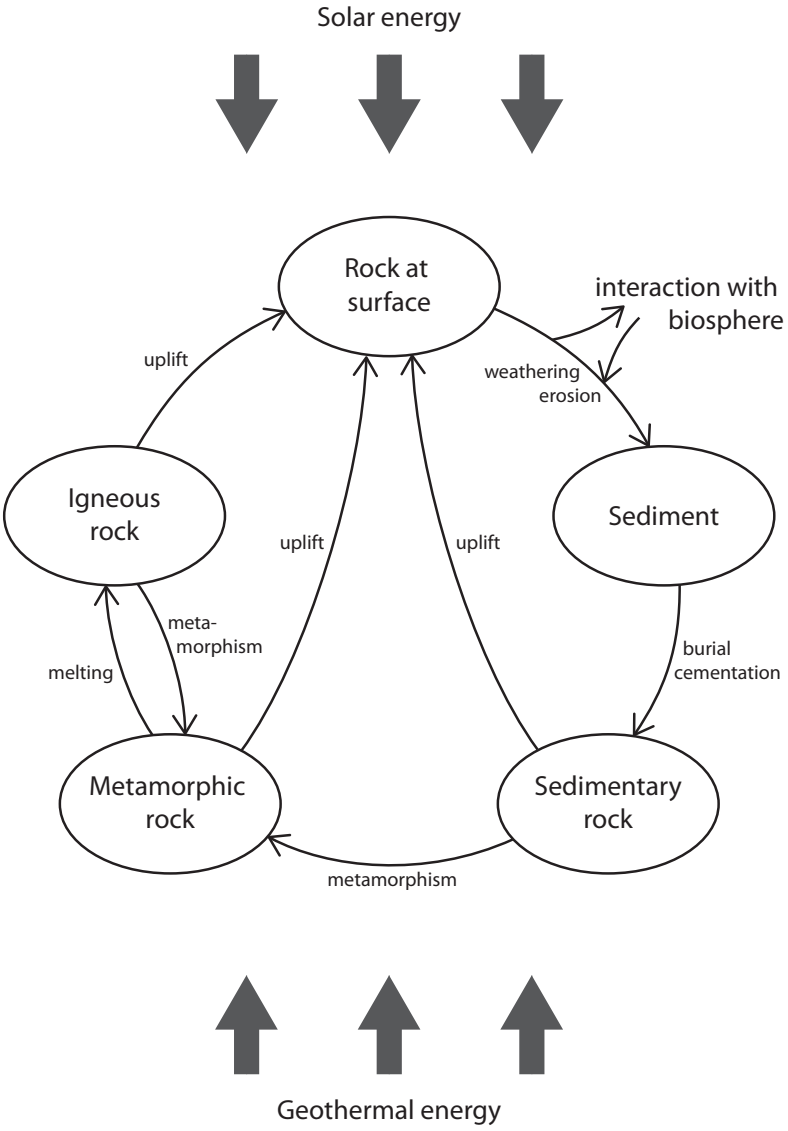

Figure 1.1: The rock cycle.

curiosity and offer a pathway for gaining a deeper understanding of processes in nature. Understanding the formation of a particular weathering morphology requires knowledge of the principal mechanisms involved in the weathering process. By understanding the process behind the weathering patterns on Earth, we may infer something about processes and conditions in distant places such as Mars and other planets [4, 5].

Weathering takes place through chemical, mechanical and biological processes (Figure 1.2). Chemical weathering includes the dissolution of unstable minerals and precipitation of stable phases, and takes place when mineral surfaces are exposed to water containing dissolved chemical species.

During mechanical weathering, intact rock is broken into smaller pieces. Perhaps the most important physical weathering processes is abrasion, which is the frictional scraping of intact rock by moving particles during erosion due to ice, water, wind or gravity. Fracturing and physical breakdown may also take place due to tectonic processes, thermal stresses, expansion due to unloading and the hydraulic action of waves, or when stresses build up in pores due to the growth of ice, salt crystals or other minerals.

Biology affects rock weathering through both chemical and mechanical processes. Dissolution and precipitation can be controlled by organic acids excreted by microorganisms, fungi, lichen or plant roots. Tree roots may expand to wedge open preexisting fractures in rocks (Figure 1.2b). The extent to which microfractures can be opened by plant roots or fungal hyphae is not yet known [6, 7].

Mechanical and chemical weathering are coupled processes. When rocks are broken, new surfaces are formed, which may be exposed to water and allow for increased chemical weathering. Fractures also act as efficient pathways for transport of water and dissolved species. In addition, chemical reactions may change the stress state in the rock in such a way that new fractures are formed (see Figure 1.3).

Because weathering rates are important for the evolution of global climate, considerable effort is being spent on models that describe the different stages of weathering as well as the propagation rate of the weathering front (the zone above the intact bedrock where weathering reactions are active) and the erosion of the top surface of the Earth. These models need to include a basic understanding of transport, kinetic processes and the coupling between mechanical and chemical processes [8–12].

During weathering, processes on the scale of outcrops and landscapes may be controlled by processes that operate on the pore scale or below. For instance, overall weathering rates can be controlled by the kinetics of the mineral-fluid interface reactions [13]. In other cases, the rate limiting step is transport, which takes place in large scale fractures as well as in

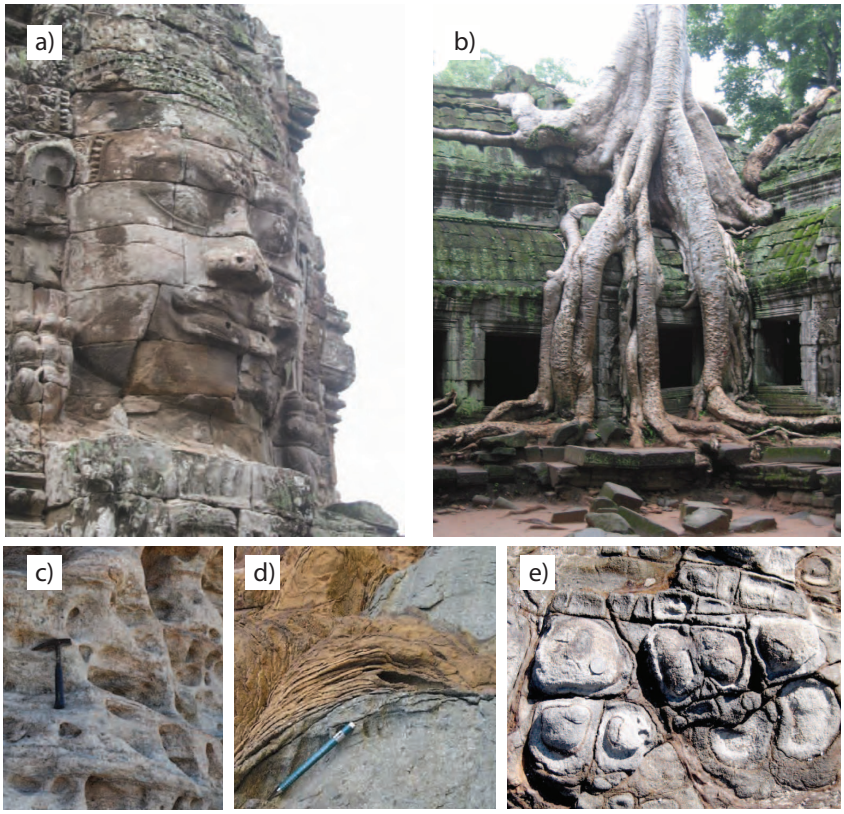

Figure 1.2: Weathering morphologies. a) This face on Angkor Wat (Cambodia) has been affected by chemical (colour changes, dissolutional rounding of sharp angles) and mechanical (flaking, and possibly some granular disintegration leading to rounding of edges) processes. b) An extreme example of biological weathering at Angkor Wat. c) Tafoni structures, Argentina (picture courtesy of Bjørn Jamtveit). d) Spalling of corners during spheroidal weathering, Puerto Rico (picture courtesy of Ray Fletcher) e) Spheroidal weathering patterns, Australia (picture courtesy of Andrew Putnis).

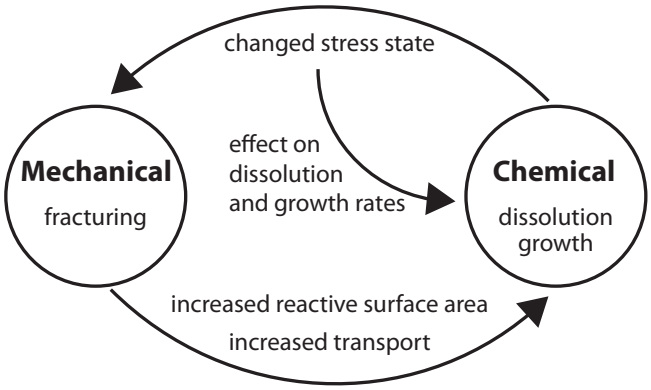

Figure 1.3: Feedback between mechanical and chemical weathering processes. Fracturing may increase the reactive surface area and transport of reactive species, thereby accelerating the chemical processes. Dissolution and growth may change the stress state of the rock in such a way that fractures form. There is also a feedback between the state of stress of a solid surface and the dissolution or growth of that surface.

confined fluids at grain boundaries. The rate limiting step can vary across the weathering profile depending on the local permeability and chemistry [13, 14]. Laboratory studies are performed to investigate the dissolution rates of rock forming minerals, and progress is being made on how to reconcile field and laboratory data [15, 16]. On the outcrop scale, several field studies indicate that the velocity of the weathering front is constant in time [17–19]. Constraints on large scale rates of erosion and weathering front propagation are obtained through isotope measurements [20–22].

In this thesis, the focus has been on stress generation due to chemical weathering processes and how this is coupled to fracture propagation both on the pore and outcrop scale. Particular emphasis has been placed on the interplay between kinetic processes at the crack tip and on the crystal surface.

The basic physics of stress generation due to crystallization and slow fracture propagation are introduced in Chapters 2 and 3. The coupling of these processes is discussed in Chapter 4. In Chapter 5 the principal findings are summarized and some reflections are made on issues which need to be addressed in future studies. The main results of this study consist of the four scientific papers included at the end of the thesis. In each of the introductory chapters, the relevant results from the papers are presented and placed in context. Figure 1.4 gives an overview of the processes and mechanisms discussed in this thesis.

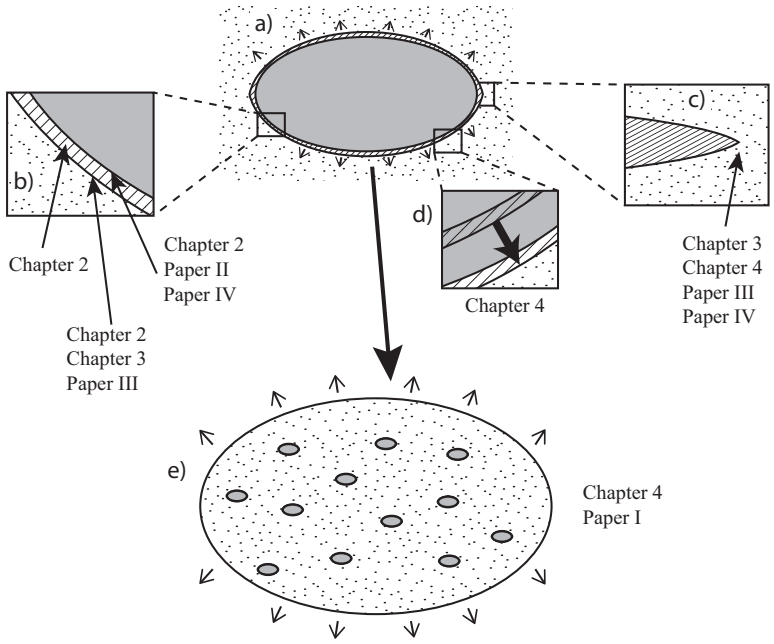

Figure 1.4: Overview of processes which are discussed in this thesis. a) Stresses generated due to crystal growth from a supersaturated solution in a pore. b) Close-up on the crystal-pore wall interface, where important processes and properties are crystal growth in the direction of normal stress (Chapter 2, Paper II, Paper IV), liquid film where normal stresses are sustained by the disjoining pressure (Chapter 2) and the energy of a solid-liquid interface (Chapter 2, Chapter 3, Paper III). c) Crack propagation (Chapter 3, Chapter 4, Paper III, Paper IV). d) Replacement (Chapter 4). e) Large-scale build up of elastic strain energy (Chapter 4, Paper I).

Chapter 2

Generation of stresses due to crystal growth

Crystallization refers to the precipitation of a structured solid from a melt or a solution. The focus of this chapter is crystallization from solutions because this is the most common situation in weathering processes, with the exception of frost damage.

The driving force for crystallization depends on a number of parameters including subcooling (for melts) or supersaturation (for solutions), temperature, hydrostatic pressure and surface normal stress. Given the appropriate conditions, it may be energetically favourable for a crystal to grow on a face which is in close contact with a confining surface, and thereby perform mechanical work by "pushing" on the surrounding matrix. The result is that crystals may "wedge" themselves into rocks to propagate fractures and produce damage through frost heave, salt weathering and the like. The stresses generated in this context are often referred to as "the force of crystallization" or "crystallization pressure".

Crystallization from solutions and from melts have much in common, but are also different in some respects. The main difference is that transport of heat and fluid advection are important in the latter case, while diffusional transport of dissolved species tends to govern the former. Stress generation due to ice growth in pores is discussed in abundant literature [23–30].

Work generated by growing crystals was first reported by Lavalle in 1853 [31], who noted that crystals growing from solution were able to push themselves upwards. Later Becker and Dey [32] (see Figure 2.1) and Taber [33] demonstrated that growing crystals could lift considerable weights. The only quantitative measurements were made by Correns and Steinborn [34], who found an agreement with their derived equation for equilibrium crystallization pressure. It has, however, been pointed out that the equation used by

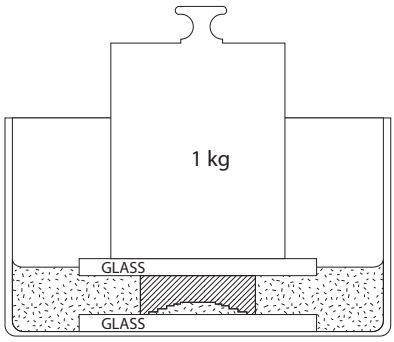

Figure 2.1: Experimental setup used by Becker and Dey [32]. A 1 cm wide crystal of alum placed between two glass plates is loaded with a 1 kg weight. The crystal is immersed in a solution of alum which is supersaturated due to evaporation.

Correns and Steinborn is off by almost a factor two due to neglecting the number of ions in the dissolved salt (see Section 2.1.2) and the effects of non-ideality. This factor is larger than the uncertainty in the reported data, something which casts some doubts on the interpretation of his quantitative results [35].

It was postulated by Correns [34], and has also later been assumed, that in order for crystallization to take place in the direction of normal load, there must be a liquid film present between the loading surface and the crystal. Without this film, there would be no material transport to the growing surface (solid diffusion is orders of magnitudes too slow for the situations we are considering), and the crystal could not grow. The existence of this liquid film is discussed in more detail in Section 2.2.

2.1 Thermodynamics of stressed crystal surfaces in contact with their solution

The thermodynamic equilibrium of a non-hydrostatically stressed solid with its solution was first considered by Gibbs [36] and later elaborated by, among others, Paterson [37], whose derivations are followed in this section.

The solubility of a solid is controlled by a number of parameters, such as temperature, pressure, surface stress and presence of other species in the

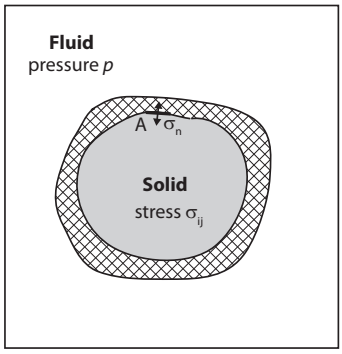

Figure 2.2: Schematic representation of closed system containing a solid under stress σ_{ij} and a fluid under pressure p in which the solid can dissolve. The stress is applied on the solid by a permeable loading frame (hatched). Figure after Paterson [37].

liquid. It can be quantified by considering the chemical potential μ of the surface of the solid as a function of these parameters, defined by the Gibbs relation $\mu_i = \frac{\mathrm{d}}{\mathrm{d}N_i}(U - TS + pV)$ where U is internal energy, T is temperature, S is entropy, p is pressure and V is volume. According to the laws of thermodynamics, a system will always evolve towards a state of equilibrium, where the chemical potentials of all components and at all positions are equal. However, different components of the system will evolve at different rates. In a situation involving the chemical equilibrium between a solid and a fluid, it is enough to consider the chemical potential of the surface, as the interior of the solid is dependent on solid diffusion and will take a much longer time to equilibrate. As liquid diffusion is much faster, all of the fluid in the system needs to be considered.

The equilibrium of a solid subject to a surface normal stress which is different from the fluid pressure can be investigated in the model system shown in Figure 2.2. The system consists of a container with a solid immersed in a fluid of constant pressure p. Stress is applied on the solid by a permeable loading frame. The solid is soluble in the fluid, and the solid component in the fluid is initially in equilibrium with the solid state. A small reversible change is then made which consists of the following steps:

1. m units of solid is detached from the surface of the solid at site A, where the component of stress normal to the surface is σ_n, and removed from the system. This changes the internal energy of the system by $-u_\sigma m$,

where u_σ is the specific internal energy of the stressed solid.

2. The loading frame is adjusted to regain contact with the surface of the solid. The change in potential energy of the loading frame (which is part of the internal energy of the system), is $p\mathrm{d}V = -(\sigma_n - p)v_\sigma m$, where v_σ is the specific volume of the solid in its stressed state.

3. m units of the component of the solid is introduced to the system in the same state as it occurs in the solution, and dispersed in the solution in the vicinity of A. The change in internal energy of the system is $u_L m$, where u_L is the partial specific internal energy of the component of the solid in the solution.

4. A different volume is occupied by m units of solid and m units in the solution. To accommodate this, the walls of the container have moved. Moving the walls back to their original position requires a work of magnitude $p\mathrm{d}V = p(v_L - v_\sigma)m$ where v_L is the specific volume of the solid component in solution. This ensures that no external work is done on the system, since the boundaries remain stationary.

5. Since the entropy of the system has changed by $\Delta S = -s_\sigma m + s_L m$ where s_L and s_σ are specific entropies of the stressed solid and solid in solution, we must add a quantity of heat equal to $-T(s_L - s_\sigma)m$ to ensure that the entropy of the system is unchanged.

As there is no change in entropy, and no work is done on this closed system, the change in internal energy is zero. This gives the following equilibrium condition:

$$-u_\sigma - (\sigma_n - p)_\sigma + u_L + p(v_L - v_\sigma) - T(s_L - s_\sigma) = 0, \tag{2.1}$$

Rearranging to get solid and liquid properties on either side of the equality, this becomes

$$u_L - Ts_L + pv_L = u_\sigma - Ts_\sigma + \sigma_n v_\sigma. \tag{2.2}$$

It follows from the Gibbs relation that the expression on the left hand side equals the chemical potential of the component of the solid in solution, μ_L. The equilibrium condition for a stressed solid and its solution in the vicinity of the stressed surface is therefore

$$\mu_L = u_\sigma - Ts_\sigma + \sigma_n v_\sigma. \tag{2.3}$$

From the theory of solutions, the chemical potential of a solute in solution is given as

$$\mu \equiv \mu^*(p, T) + kT \ln a \tag{2.4}$$

where k is the Boltzmann constant. μ^* can be taken as a constant in our case, since it is a function of pressure and temperature only, and a is defined as the activity of the solute. This gives

$$\mu^*(p,T) + kT \ln a_\sigma = u_\sigma - Ts_\sigma + \sigma_n v_\sigma \tag{2.5}$$

where a_σ is the activity of the component in solution in equilibrium with the solid under normal stress σ_n. In a hydrostatic condition, where $\sigma_n = p$, this would give

$$\mu^*(p,T) + kT \ln a_p = u_p - Ts_p + pv_p. \tag{2.6}$$

Combining these equations gives us the following equilibrium condition:

$$kT \ln \frac{a_\sigma}{a_p} - [(u_\sigma - Ts_\sigma) - (u_p - Ts_p)] - \sigma_n(v_\sigma - v_p) + (\sigma_n - p)v_p = 0. \tag{2.7}$$

The $u - Ts$ terms represent the difference in elastic strain energy between the solid under stress and at hydrostatic pressure, while the $\sigma_n(v_\sigma - v_p)$ term is the contribution from the differences in specific volumes, which is also a consequence of elastic strain. These terms will normally be much smaller than the last term, unless $\sigma \approx p$, which can be the case for the free face of a uniaxially stressed crystal. We will therefore for now turn our interest to the case where $\sigma_n \gg p$. To simplify, we introduce the deviatoric stress $\sigma_c = \sigma_n - p$. We will also assume that the solute activity and specific volume at hydrostatic pressure p are very close to those of some reference state, so that we can replace a_p and v_p with a_0 and v_0 to get

$$kT \ln \frac{a_\sigma}{a_0} - \sigma_c v_0 = 0. \tag{2.8}$$

This equation is a condition for equilibrium. It tells us that in every solid-liquid system, the solid will neither grow nor dissolve when the deviatoric surface normal stress equals σ_c, provided that the solute activity of the fluid in the immediate vicinity of the stressed solid is a_σ. If the equality is replaced with $>$, the crystal will tend to grow; in the opposite case, it will tend to dissolve.

2.1.1 Effect of surface tension, and a possibility of sustaining large stresses at equilibrium

For very small crystals ($\lesssim 0.1\ \mu$m), an extra term is needed in the equilibrium condition to account for the energy cost of creating new surface area [38]:

$$kT \ln \frac{a_\sigma}{a_0} - \sigma_c v_0 - \gamma_{cl} v_0 \frac{\mathrm{d}A}{\mathrm{d}V} = 0, \tag{2.9}$$

where γ_{cl} is the surface energy of the crystal in the liquid. As this last term is larger for smaller crystals, they are in equilibrium with solutions of higher solute activity than larger crystals. This corresponds to a higher solubility (higher equilibrium fluid concentration) in small pores, which has been demonstrated experimentally [39].

If a large crystal is loaded on two faces, while the other faces remain free, the chemical potential will be higher on the loaded faces than on the free faces. Growth can take place on all faces given that the solution activity is sufficiently high, but if the system is closed, the activity of the solution will become lower as material is removed from solution to be incorporated in the crystal. When the free faces reach equilibrium with the bulk solution, the chemical potential of the loaded faces is such that they will tend to dissolve. It is therefore not easy to envisage an equilibrium situation where a high crystallization pressure is maintained through time. If the system is completely saturated with fluid, a possible solution is to consider cylindrical pores, or circular pores with small entrances, where the geometry of the pore can be such that the free faces of the crystal will attain an equilibrium curvature which is higher than the curvature of the loaded faces, and hence be in equilibrium is reached with a fluid which on the loaded faces has a high enough activity to allow for some sustained stress [26, 40].

2.1.2 Calculation of solution activity

The degree of supersaturation of the fluid is described in terms of the activity ratio as in Equation (2.8), but depending on the nonideality of the fluid the calculation of the exact value of the activity can be quite complex. For nonhydrous salts of low solubility, it is sufficiently accurate to neglect the non-ideal behavior of water and the water component of hydrated salts, which yields the following approximation [40]:

$$kT \ln \frac{a_\sigma}{a_0} = nkT \ln \Omega, \tag{2.10}$$

where n is the total number of ions released upon complete dissociation of the salt, and $\Omega = c/c_0$ is the solution supersaturation. More accurate expressions are given by Steiger [40].

2.2 Confined fluid films

In order for a liquid film to exist between two solid surfaces subject to a deviatoric surface normal stress σ, force balance requires the pressure p_f in

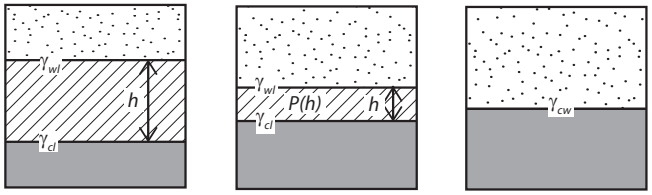

Figure 2.3: Energy of a film between two solid surfaces. Left: In a thick film the associated energy is the sum of the two solid-liquid interfacial energies γ_{cl} and γ_{wl}. Middle: For thin films there is an additional energy term $P(h)$ which depends on the separation h. Right: When the film thickness goes to zero, the energy is that of the dry solid-solid interface γ_{cl}.

the liquid film to be $p_f = \sigma$ and consequently higher than the hydrostatic pressure p of the bulk fluid. This elevated pressure is often referred to as the disjoining pressure of the thin film.

The disjoining pressure can be derived from a macroscopic continuum picture by considering the interfacial energies of solid-liquid and solid-solid interfaces or a microscopic continuum model where the interaction forces between two surfaces separated by a liquid are considered; both of these methods yield consistent results. The theory, as described in the following subsections, is well established for static interfaces. If one interface is moving, as may be the case when a crystal is growing against a load, there may be additional effects which come into play.

2.2.1 Surface energies and disjoining pressure

This section follows the derivations by de Gennes *et al.* [41].

Consider a crystal growing in a pore, where the crystal surface is separated from the pore wall surface by a thick (thickness $h \gg 100$ nm) film of liquid. The energy of the thick film is given by the sum of the crystal-liquid and wall-liquid interfacial energies, $U_\infty = \gamma_{cl} + \gamma_{wl}$ (where the energy U in this case is defined per unit area). If the surfaces are moved progressively closer to each other so that the film becomes very thin ($h \to 0$), the energy must become that of the dry solid-solid interface, $U_0 = \gamma_{cw}$ (Figure 2.3).

For intermediate film thicknesses, a thickness dependent energy $U(h)$ can be assigned by introducing some function $P(h)$ to get

$$U(h) = \gamma_{cl} + \gamma_{wl} + P(h), \tag{2.11}$$

with the boundary conditions $P(\infty) = 0$ and $P(0) = \gamma_{cw} - (\gamma_{cl} + \gamma_{wl})$.

If the thickness of the film is increased by an amount $\mathrm{d}h$ by adding $\mathrm{d}N$ molecules, then $\mathrm{d}N = \mathrm{d}h/v_0$ where v_0 is the specific volume of the molecule in the liquid phase. The energy of the film is changed by an amount $\mu_f \mathrm{d}N$, where μ_f is the chemical potential of the liquid in the film, which includes an additional term to the reference chemical potential μ^* of the bulk liquid to account for the change in $P(h)$:

$$\mu_f \mathrm{d}N = \mu^* \mathrm{d}N + \frac{\mathrm{d}P}{\mathrm{d}h}\mathrm{d}h. \tag{2.12}$$

We can then define the disjoining pressure $\Pi(h)$ by

$$\Pi(h) \equiv -\frac{\mathrm{d}P}{\mathrm{d}h}. \tag{2.13}$$

Combining these two equations reveals that the disjoining pressure is related to the chemical potential through

$$\mu_f = \mu^* - v_0 \Pi(h). \tag{2.14}$$

This shows that if the disjoining pressure is positive, the chemical potential of the film becomes lower than that of the bulk liquid, which will act as a driving force for fluid migration against the positive pressure gradient and into the thin film. Equilibrium with the bulk fluid is reached when $\mathrm{d}P/\mathrm{d}h = 0$.

2.2.2 Surface forces

The interaction energy between surfaces separated by a liquid by more than a few molecular diameters is determined by long range van der Waals and electrostatic forces. The non-retarded van der Waals interaction energy between two planar surfaces separated by a liquid film of thickness h follows the dependence [42]

$$U_{vdW} = -\frac{A_H}{12\pi h^2}, \tag{2.15}$$

where the Hamaker constant A_H describes the interaction of the particular materials involved. For interactions across a water film, the Hamaker constant is typically positive, which means that the resulting van der Waals forces are attractive and increase with decreasing separation.

Electrostatic forces arise between surfaces in a liquid due to the build-up of so-called electric double layers (DL) due to the balancing of surface charges

by ions in solution. For planar surfaces the interaction energy related to this process depends exponentially on the separation distance, [42]

$$U_{DL} \propto \frac{1}{\lambda_D} \mathrm{e}^{-h/\lambda_D}, \tag{2.16}$$

where the length scale is given by the Debye screening length λ_D, which is a function of the electrolyte concentration of the fluid. In ultra pure water, λ_D is close to 1 μm, while in concentrated solutions it is on the order of a few Å.

The so-called DLVO theory [42], named after Derjaguin and Landau [43] and Verwey and Overbeek [44] which approximates the net force acting between the surfaces to be the sum of these two forces, provides a good qualitative understanding of how the interaction energy varies with separation and electrolyte concentration (Figure 2.4). At very short separations, the attractive forces always dominate (provided that the Hamaker constant is positive) implying that if surfaces are brought sufficiently close together, they will form a strong, dry adhesive contact. Since the van der Waals interactions are largely insensitive to electrolyte concentration while the range and magnitude of the electrostatic interactions are strongly dependent on electrolyte concentration, the qualitative result of the combination of these two forces depends on the electrolyte concentration. For low concentrations, repulsive forces dominate up to very large separations. As the concentration is increased, repulsive forces only dominate for some intermediate range of separations, before at very high concentrations the repulsive contribution becomes negligible. In this case, the solid surfaces will be forced into contact and no disjoining pressure develops in the film. In the cases where there is a repulsive region, there exists a repulsive energy barrier which must be overcome in order to bring the dry surfaces into contact. The force needed to overcome this barrier defines the maximum disjoining pressure which can develop in the thin film. If the normal stress across the two surfaces is larger than the maximum disjoining pressure, then the liquid film will be displaced.

While the DLVO theory is a good qualitative explanation for many phenomena in colloid and surface science, it is often not sufficient for making quantitative predictions. Experimental measurements are necessary for obtaining quantitative data on the forces between surfaces of different materials and in different liquids. Measurements are typically made using the surface forces apparatus (SFA) [45] or by atomic force microscopy (AFM). Some measurements for geologically relevant systems are described by references [46–48].

For surface separations less than about 2 nm, the interaction energy is dominated by effects related to the discrete molecular nature of the surfaces,

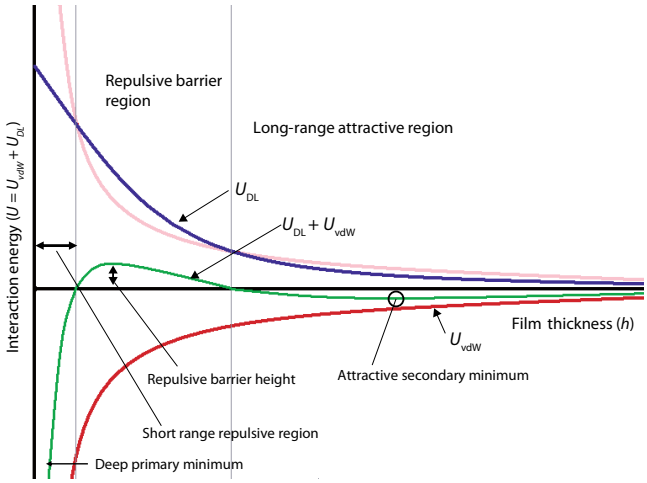

Figure 2.4: Conceptual figure of the interaction energy of two surfaces separated by a fluid film of thickness h as described by DLVO theory (Figure courtesy of Paul Meakin). The blue line shows the repulsive screened electrostatic interactions, which decay exponentially with film thickness. The attractive van der Waals interactions, which follow an inverse power dependence of film thickness, are shown as the red line. In DLVO theory, the total interaction energy is given by the sum of these two interactions. As a guide to the eye, the pink line shows the negative of the van der Waals interaction energy. In the situation shown, attractive forces dominate at long and very short separations, while there is an intermediate range where the repulsive forces dominate. A repulsive barrier must be overcome in order to bring the two surfaces into contact at the deep primary minimum.

solvent and ions [45, 46, 49, 50], which are not accounted for in the continuum DLVO theory. At least in the case of mica surfaces (which have been most commonly used in SFA experiments), "steric-hydration" forces between surfaces with a strongly bound layer of water molecules give rise to disjoining pressures of more than 100 MPa for concentrated solutions, while DLVO theory can account for pressures on the order of 1 MPa [46].

2.3 Thesis results

2.3.1 Interface structure

Consider a crystal in contact with a supersaturated solution and loaded by a heavy weight on the top face such as in the setup by Becker and Dey (Figure 2.1). If the crystal face in contact with the glass plate is initially rough, then the stress distribution on the crystal face will range from very high in the areas closest to the glass plate, to essentially zero in portions which are further away. From a continuum perspective, because the equilibrium supersaturation is higher for surfaces subject to a large normal stress (Equation (2.8)), we would expect portions of the surface subject to a high normal stress to grow much more slowly than unstressed portions of the surface, or even to dissolve if the local stress is higher than σ_c. With time, this would cause the surface to become smooth and the stress on the crystal face to become evenly distributed (assuming that the loading surface is a perfectly smooth plane).

The growth rate of a crystal surface may be limited by growth kinetics, transport, or both. If a crystal face is separated from the loading surface by a liquid film of only a few nanometer thickness (which is required for the disjoining pressure to be sufficient to transmit the normal stress between the surfaces [47]), it is reasonable to assume that growth is limited by transport, since the diffusion current, which is proportional to the film thickness, will be very small in this case. Weyl [51] analyzed this situation for a cylindrical crystal with a normal stress applied to its circular face, and calculated the rate of growth in the direction of load as a function of stress and bulk supersaturation. Weyl's study is one of very few dynamic models of this sort of process, and is extensively cited in papers dealing with stress generated by crystallization.

In addition to calculating growth rates, the model also predicts that for mean applied stresses up to half of the equilibrium stress σ_c, growth should only take place on a rim surrounding a hollow core. Growth rims are commonly found on crystals grown from solution while resting on the bottom of

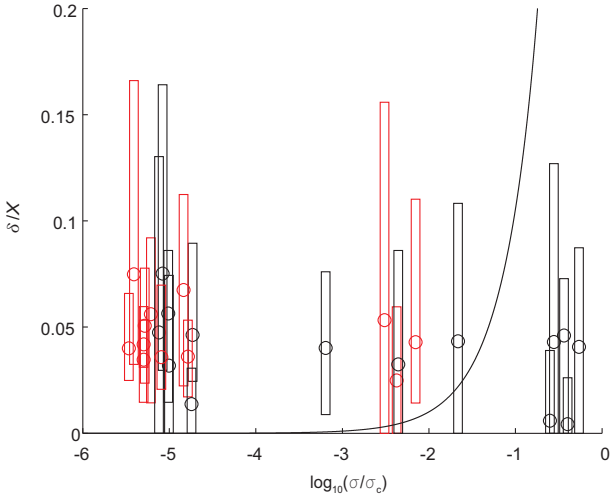

Figure 2.5: Measured growth rim widths as a function of applied normal stress (see Paper II). The prediction from Weyl's model is shown as a solid line.

a dish, and they were also reported and discussed by Becker and Dey [32, see also figure 2.1] and Taber [33].

Paper II describes experiments which have been performed in order to test the growth rim predictions by Weyl. The initial motivation was to use these results to infer how the thickness of the liquid film was related to applied stress and solution saturation. However, surprisingly, the measured growth rim widths showed none of the dependencies given in Weyl's model (Figure 2.5). The reason for this became evident upon examining the surface morphologies of the growth rims. They are in fact very rough with topological features which are several μm in height (Figure 2.6). The contact between the rim surface and glass cannot therefore be assumed to be smooth, which violates the basic assumption of Weyl's model.

It was found that the rims on the loaded faces most likely develop due to a step bunching instability due to much more rapid growth along the edges than in the central portion of the confined face. This happens due to a strong concentration gradient parallel to the confined face which develops as a consequence of the balance between diffusional transport from the bulk

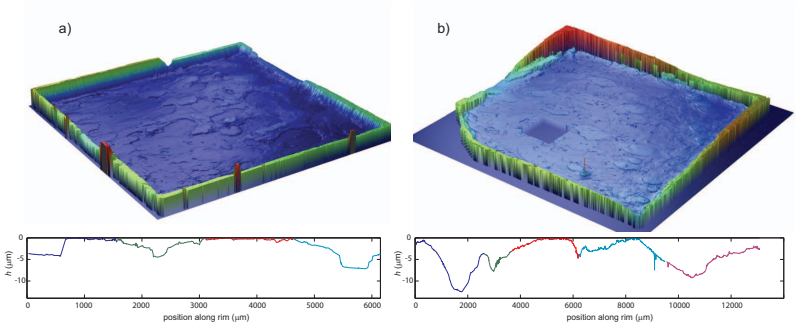

Figure 2.6: Topographies of two loaded crystal faces measured at the end of the experiment. The crystal in a) has been growing under its own weight while that in b) was loaded by a 200g calibration weight. The line plots show a 2D transect along the rim; different sides are marked by different colors. The h scale shows the inferred distance from an imagined glass plate.

solution and removal of ions due to surface growth.

In the context of pressure solution, which can be viewed as the inverse process of the force of crystallization [51], the structure and transport properties of the interface have been investigated in some detail. Since observed rates of solution compaction are much larger than what can be explained by diffusion through a smooth thin film [46], various models for rough interfaces have been proposed, where diffusion through regions of thicker films allows for increased transport. Some degree of interfacial roughness has been confirmed by experimental studies [52–54]. The results from Paper II suggest that these considerations may also be valid in the context of the force of crystallization.

2.3.2 Surface energy of calcite

An equilibrium thermodynamic requirement for a liquid film to exist between a crystal face and a confining wall is that the sum of the solid-fluid interfacial energies for the crystal and wall does not exceed the energy of a dry crystal-wall interface; otherwise it may be energetically favourable for the system to expel the liquid to produce a dry contact. This can be expressed as

$$\gamma_{cw} > \gamma_{cl} + \gamma_{wl}. \tag{2.17}$$

If a crystal is growing in a pore where the above requirement is not fulfilled, it would be expected to grow into dry contact with the pore wall rather than maintaining a liquid film, and hence no stress would be exerted on the pore wall. While this is useful as a conceptual criterion for whether stresses can be generated during crystallization, it is less useful in practice due to the limited availability of high quality data on interfacial energies.

The energies of mineral-fluid interfaces are typically found from numerical simulations or from precipitation studies. An alternative and less used method is to infer the surface energies from the lower energy threshold for subcritical crack propagation. In Paper III, this method has been used to measure the surface energy of the $\{10\bar{1}4\}$ cleavage plane of calcite as a function of water concentration (Figure 2.7). Our results agree well with previous experiments in dry and water saturated conditions. As was also found in molecular dynamics simulations, the effect of increased water concentration is an almost linear decrease in surface energy.

Damage due to salt crystallization in calcite bearing building stones such as limestone is an important engineering problem. For future studies, it would be useful to investigate how the surface energy of calcite is affected by the concentration of some common salts. This would have implications both for the stress exerted by salt crystals on calcite surfaces, and also on possible opening and propagation of fractures in calcite, which is further described in Chapter 2.

2.3.3 Stress evolution through time: Effect of boundary conditions

Equilibrium thermodynamics can be used to predict the maximum normal stress which can be sustained by a crystal surface before it will start to dissolve. It is often assumed that when a supersaturated solution is introduced to a porous medium, the mean pressure which is generated in large pores can be found from Equation (2.8) or that it is given by the pore geometry (see Section 2.1.1).

However, it may take a long time before equilibrium is reached, and fractures may initiate and propagate while the system is still far from equilibrium. The time evolution of crystallization stresses may be coupled to kinetic fracture propagation (See Chapter 3) and to transport within the porous medium. Knowledge about the dynamics of stress generation due to crystallization may therefore be important for understanding how rocks are damaged due to crystallization stresses.

The stress on the pore wall is generated by the growing crystal and is

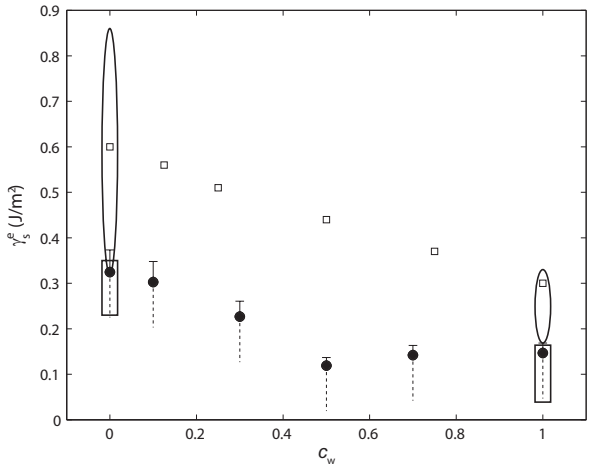

Figure 2.7: Surface energies γ_s^e of calcite as function of water concentration (mole fraction or surface cover fraction). Filled circles are estimates from experiments on calcite (this study). The measured γ_s^e are plotted with asymmetric error bars: The upper shows the experimental uncertainty, while the lower is undefined, indicating that our values represent upper bounds. Open squares are surface energies for calcite surfaces with partial coverage of water, calculated by atomistic simulations [55]. Ellipses show the range of numerical results from literature for dry and wet calcite surfaces, while rectangles show the range of experimental results from literature (see Paper III).

initially zero before the crystal comes into contact with the pore wall. As the crystal is growing into contact with the wall, the growth rate of the crystal decreases with increasing stress until it reaches zero when $\sigma = \sigma_c$. The rate of stress generation is determined by the compliance of the pore, which describes the magnitude of stress needed for a given displacement of the pore wall.

In Paper IV, the evolution of normal stress σ for a crystal growing in the aperture of a penny shaped crack (Figure 4.2b) has been analyzed. One outcome of this model is shown in Figure 2.8. Two results from the analysis are worth mentioning in the context of this chapter. The first is that the stress on the crystal face only asymptotically approaches σ_c, with a time scale determined by the pore compliance and the kinetic constant and specific volume of the crystal. This is a general observation which should hold for any pore geometry, provided that the supersaturation of the solution is constant. The second observation is that if fractures develop, the fracture velocity has a direct control on the stress on the crystal face due to the change in fracture compliance.

The discussion of fracture evolution in this model is presented in Chapter 4.

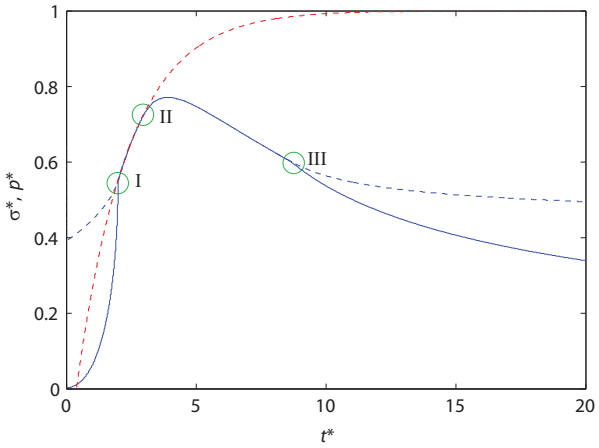

Figure 2.8: Evolution of normal stress ($\sigma^* = \sigma/\sigma_c$) on the confined crystal face in a penny crack (see Figure 4.2b) as a function of nondimensional time (see Paper IV) for a crystal growing from a constant supersaturation. The dashed blue line shows the normalized stress on the crystal face. The effective pressure p^*, which denotes the fluid pressure which would be required to maintain the observed energy release rate of the crack, is shown as the solid blue line. The red dashed line shows the asymptotic increase in stress which is predicted for a stationary, filled crack. The crystal nucleates in the center of the fracture with initial opening close to zero. The stress on the crystal face which comes into contact with the crack wall is initially larger than the effective pressure, but both the effective pressure and the crystal stress approaches the asymptotic solution as the crystal grows to fill more of the crack. At point I, the crystal fills the entire fracture ($a = c$). Crack propagation is initiated at point II, and because the fracture compliance increases with crack length, σ^* and p^* decrease as the fracture grows. From III the velocity of the crack tip is faster than the growth rate of the free crystal face, so that $a < c$. As the crystal area supporting the load becomes smaller relative to the fracture size, the stress on the crystal face increases. For further details and a full description of the model, see Paper IV. The dimensionless parameters used to generate this plot are $A = B = C = 1$ and $c_0^* = 2$.

Chapter 3

Fracture mechanics and kinetic fracture processes

3.1 Basic fracture mechanics: Griffith theory

The basis of today's fracture mechanics theories were established in the 1921 paper by Griffith [56]. At that time, the prevailing notion was that rupture should be controlled by the maximum elastic stress or strain which could be sustained by a material. On the other hand, experiments showed a clear relationship between scratch sizes and strength in rupture tests. In the search for a theory to explain these observations, Griffith chose the thermodynamics approach to a fractured system. He made use of the derivations of Inglis [57], who had shown that the strain energy associated with a crack subject to a remote stress is proportional to the square of the crack length. A thermodynamic rupture criterion would imply that for rupture to have taken place, the system must have passed from the unbroken to the broken state through a continuous decrease in the total energy of the system, which also includes the energy of the two newly surfaces. In order to consider crack surfaces of sufficient separation to ignore cohesive forces between the crack surfaces, and to assess incremental crack advancements, Griffith's starting scenario was a body with a preexisting crack of a size fulfilling these requirements. The equilibrium condition for a crack is then given as

$$\frac{\delta}{\delta c}(U_M - U_S) = 0, \tag{3.1}$$

which means that for an incremental change of the crack length c away from equilibrium, the change in mechanical energy U_M exactly matches the change in surface energy U_S. This very powerful statement defines how fracture propagation is understood today.

The mechanical energy of the system can be described by the mechanical energy release rate $\mathcal{G}$ (this is not a rate defined with respect to time, but rather a mechanical energy defined per unit length of the crack front), defined as [58]

$$\mathcal{G} \equiv -\frac{\mathrm{d}U_M}{\mathrm{d}c} \tag{3.2}$$

The criterion for crack propagation then becomes

$$\mathcal{G} > \frac{\mathrm{d}U_S}{\mathrm{d}c}.$$

The mechanical energy release rate $\mathcal{G}$ is theoretically defined for a range of idealized crack geometries. It is related to the stress intensity factors $K_\mathrm{I}, K_\mathrm{II}$ and K_III, which are commonly used in engineering, through

$$\mathcal{G} = \frac{K_\mathrm{I}^2}{E'} + \frac{K_\mathrm{II}^2}{E'} + \frac{K_\mathrm{III}^2(1+\nu)}{E}, \tag{3.3}$$

where $E' = E$ for plane stress and $E' = E/(1-\nu^2)$ for plane strain, and ν is Poisson's ratio. The subscripts I, II and III refer, respectively, to pure tension, in-plane shear and anti-plane shear loading.

The change in surface energy U_S with crack extension can be related to the intrinsic surface energy γ of the material through [59]

$$2\gamma_s = \frac{\mathrm{d}U_S}{\mathrm{d}c}. \tag{3.4}$$

This is a measure of the energy required to break bonds in order to create two new surfaces as the crack extends. γ_s is defined as energy per unit area. Within this framework, we would expect the crack to extend if $\mathcal{G} > 2\gamma_s$, and to heal if $\mathcal{G} < 2\gamma_s$.

3.2 Effect of the environment

After the establishment of the Griffith theory, considerable effort was put into trying to resolve observations which seemed to be in disagreement with the theory. One of these was fatigue in glass, which, if loaded for long times, was observed to fail at approximately one third of the short-time breaking stress. Further allusion to a chemical effect was made in 1930 by Obreimoff's experiments on the slow fracture of mica in a controlled environment [60] .

These observations were reconciled with the Griffith theory in the 1944 paper by Orowan [61]. The change in force from vacuum to air can be related to an adsorbed film of air or moisture which lowers the effective surface energy

γ_s to a value γ_s^e which depends on the chemistry of the environment. This implies that the air molecules must be able to penetrate to the crack tip. If the crack is propagating very fast, the adsorbed film would not be able to keep up with the motion of the crack tip. The new surfaces would in effect open in vacuum, and so the vacuum surface energy γ_s should be used. If on the other hand the crack opens very slowly, the adsorbed film has time to diffuse to the crack tip, and the newly created surfaces have energy γ_s^e. This explains the apparent lowering of strength from vacuum to air.

3.3 Time effects

Both in the fatigue observations and in Obreimoff's experiment, there had been a clear indication of a time effect on the fracture process. The Griffith treatment of cracks was made only within the framework of the first law of thermodynamics, and could as such not deal with effects away from equilibrium. Rice [62] generalized the Griffith theory by considering irreversible thermodynamics. When a crack velocity v is introduced, he showed that positive entropy production with time is only maintained if

$$(\mathcal{G} - 2\gamma_s^e)v \geq 0. \tag{3.5}$$

This implies that there should exist a well defined crack velocity function $v(\mathcal{G})$ defined for some deviation of $\mathcal{G}$ from $2\gamma_s^e$, where v is positive (crack opening) for $\mathcal{G} > 2\gamma_s^e$, and negative (crack healing) for $\mathcal{G} < 2\gamma_s^e$. For large departures from equilibrium, crack propagation may become unstable. This happens as the crack velocity approaches the Rayleigh wave speed in the medium, and this dynamic fracture propagation has been studied extensively [63].

3.4 Experimental crack velocity data

Due to a number of devoted experimentalists since the middle of the 20th century, crack velocity functions $v(\mathcal{G})$ have been demonstrated for a range of materials such as mica [60, 64, 65], glass [61, 66–71], quartz [72–78] and other rock forming minerals including calcite [77], as well as polycrystalline rocks [79–83] and ceramic materials [84]. The crack velocity is often reported as a function of the stress intensity factor K_{I} (Equation 3.3). The results can generally be summarized as in Figure 3.1, where the subcritical crack growth can be grouped into three regimes I, II and III. In regime I, the velocity fits well to a power law of K_{I}, as what is now refered to as the Charles' law [85]

$$v = AK_{\mathrm{I}}^n, \tag{3.6}$$

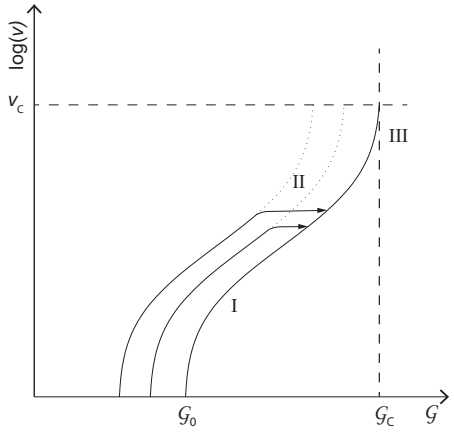

Figure 3.1: Schematic diagram of subcritical crack propagation (after Maugis [59]). The curve to the right corresponds to propagation in vacuum. As water is introduced, the threshold $\mathcal{G}_0$ becomes lower, and the whole curve is shifted left. Region I crack propagation velocity is thus highly dependent on $\mathcal{G}$ and on the environmental conditions. At some velocity, transport of chemically active species to the crack tip may become rate limiting, and the rate of crack growth becomes approximately constant (region I) until the vacuum curve is reached. Propagation near $\mathcal{G}_c$ is highly stress dependent (region III). Above $\mathcal{G}_c$ and v_c, the dynamic fracture regime is entered, where the fracture velocity does not depend on the environment because the crack tip is under vacuum conditions.

where A is some empirical prefactor and n is an exponent which is typically in the range 10-90. When very low velocities can be measured, the curve has been found to bend towards a threshold value which would represent the Griffith equilibrium at $\mathcal{G}_0$ [59, 65, 86] (see Figure 3.2). K_I gives a good fit to a power law of K_I with the exponent n in the range 10-90 [80]. While the Charles law is a useful empirical relation, no firm theories have been posed to explain the power law relationship, which is really indistinguishable from an exponential relation for the small range of K_I which can be observed (more about this in Section 3.6).

Region II is more often observed in gaseous environments, and is thought to be related to crack growth limited by the transport of environmental species to the crack tip. Crack growth in this region is relatively insensitive to $\mathcal{G}$. The $\mathcal{G}$ dependence in this region can be attributed to the increased aperture of the crack, which enhances transport.

Region III tends to fit a power law with a much higher exponent than region I, and is thought to be controlled mainly by intrinsic crack tip processes under vacuum conditions, since chemical species can no longer keep up with the propagating crack. Region III crack growth has been found to be relatively insensitive to environmental conditions, but not completely [69].

In region I, increasing the concentration or activity of water tends to give higher velocities for a given $\mathcal{G}$. The degree of influence of reagent chemistry on crack velocity is in general found to be most pronounced at low values of $\mathcal{G}$ [75]. Raising the temperature gives, in most cases, increased crack velocity [76, 80]. Changing the pH of the environment affects crack growth in a non-trivial way. For example, Atkinson [75] found that raising the pH increased crack velocity and decreased the slope of the velocity curves for quartz, so that the difference became less pronounced at higher $\mathcal{G}$-values. Dunning [77] found some weakening at high pH and strengthening at low pH in quartz, but also found no simple relationship.

3.5 Proposed mechanisms for subcritical crack growth

Much effort has gone into identifying possible mechanisms for subcritical crack growth. Sometimes this involves some confusion about the Griffith criterion, where the onset of dynamic fracture is thought to be the Griffith equilibrium point and subcritical fracture is explained as some sort of anomalous fracture which has to be explained by a different mechanism than regular crack propagation [59, 87].

Subcritical cracking in glass is perhaps the most extensively studied system in this context, and it is where the most thorough theory for the underlying mechanism is established. Charles [66] was the first to suggest a corrosion mechanism at the crack tip of glass where the strong Si-O-Si bond is replaced by a much weaker OH^+-Si bond through a reaction with water molecules. The weakening of bonds would then allow for crack growth at smaller stresses, with a velocity controlled by the reaction rate. Michalske [88, 89] developed this model by considering the bond rupture process as consisting of a three-step chemical reaction between the strained Si-O-Si bond and a water molecule. This form of stress-enhanced reaction, which may differ in glasses of different compositions [90], is now the prevailing theory for subcritical fracture of glass [91] and quartz [92].

In some experiments, a velocity plateau has appeared at low crack velocities (well below region II behaviour). It has been suggested that this shows crack growth through preferential dissolution at the crack tip, such that the crack propagation rate is controlled by the dissolution rate of the material [79, 80, 93, 94]. However dissolution and removal of material is related to blunting of the crack tip, which is in contradiction to Griffith theory where an atomically sharp crack tip is postulated [95]. AFM studies of crack surfaces have also indicated that although material may be removed behind the crack tip, the tip itself remains sharp [96].

There has been some ongoing debate about whether nanoscale plastic processes take place at the advancing crack tip in amorphous materials such as glass [97, 98], but the most current agreement is that crack propagation remains brittle, and that brittle nanocracks may open in a process zone ahead of the main crack tip [99, 100].

Surface forces or surface energy effects have been found to be relevant in many aspects. As discussed in Chapter 2, repulsive forces may be present in liquid films confined between solid surfaces at small separations. When fluids are present near the crack tip, the disjoining pressure in the fluid may effectively enhance the stress at the crack tip, thus reducing the applied mechanical energy release rate necessary for crack propagation [58]. Wiederhorn and Fuller [101] showed that surface forces associated with water trapped in a small (< 1nm) gap between the crack walls could have an important effect on subcritical fracture in glass.The charge densities of mica fracture surfaces has been shown to depend on the rate of fracture propagation [64]. In addition, the ζ-potential of the system, which is the electrostatic potential between the adsorbed monolayer on the surface of the material and a distant point in the fluid, may [102] or may not [103, 104] have an effect on crack propagation.

3.6 Reaction rate theory of slow crack growth

A system containing a crack for which $\mathcal{G} \neq \mathcal{G}_0$ may evolve towards equilibrium through crack propagation or crack healing. The rate at which the system evolves depends on the height of energy barriers which must be surpassed by some thermally activated process in order to reach an energetically lower state. Macroscopic crack advance takes place if the energy barrier for crack propagation, ΔF_+, is larger than that for crack healing, ΔF_-. The asymmetry in the forwards and backwards energy barriers is caused by the departure from mechanical equilibrium given by $\mathcal{G} - \mathcal{G}_0$.

When the departure from equilibrium is small, we can express the energy barriers $\Delta F_\pm$ as a simple Taylor expansion of the quiescent energy barrier ΔF^* through [65]

$$\Delta F_\pm = \Delta F^* \mp \alpha(\mathcal{G} - 2\gamma_s^e) + ..., (\mathcal{G} - 2\gamma_s^e \ll 2\gamma_s^e) \tag{3.7}$$

where α is an activation area and $2\gamma_s^e$ is two times the surface energy of the solid in the given environment for region I crack propagation. From classical reaction rate theory, it follows that the crack velocities in region I is given by [65]

$$v_{\mathrm{I}} = 2v_0 a_0 \exp(-\Delta F^*/kT) \times \sinh\left[\alpha(\mathcal{G} - 2\gamma_s^e)/kT\right], \tag{3.8}$$

where $v_0 = kT/h$ is a fundamental lattice vibration frequency and a_0 is some characteristic atomic spacing between successive barriers.

The velocity function for region II will depend on transport processes, and if free molecular flow is rate limiting, it will be given as

$$v_{\mathrm{II}} = \lambda p \mathcal{G}, \tag{3.9}$$

where λ is a material-geometry coefficient and p is the partial pressure of the active species [65].

In region III, the functional dependency on $\mathcal{G}$ is the same as in region I but with the vacuum surface energy instead of the environment dependent value γ_s^e and possibly with a different activation area and quiescent energy threshold.

This model gives a good fit to experimental data for a range of materials and crack velocities [105]. It has also been established that reaction rate treatment of atomistic and continuum of crack models yield consistent results [106].

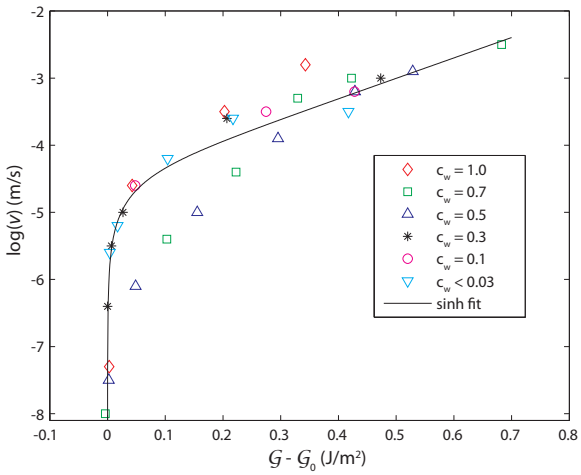

Figure 3.2: Measured fracture velocity v as a function of excess mechanical energy release rate $\mathcal{G} - \mathcal{G}_0$. The different symbols denote measurements at different water concentrations c_w. The solid line shows the results from Equation (3.8) using $a_0 = 5$ Å as a characteristic barrier spacing and with fitting parameters $\alpha = 2.0 \times 10^{-20}$ m^2 and $\Delta F^* = 7.6 \times 10^{-20}$ J.

3.7 Thesis results: Subcritical crack growth in calcite

In Paper III, measurements on subcritical cleavage crack propagation of single calcite crystals are presented. To the authors' knowledge this is the second (see [77]) experimental study of subcritical crack propagation in single calcite crystals and the first addressing the particular influence of water concentration.

Measured crack velocities were quite variable, particularly at low water concentrations and/or high $\mathcal{G}$, something which may be related to low temperature plastic behaviour in calcite. The highest velocities measured at any given $\mathcal{G}$ were assumed to correspond to the most "true" brittle crack behaviour. Within the experimental range of energy release rates and fracture velocities, the "brittle" crack velocities were found to be well described by the reaction rate model given by Equation (3.8) (see Figure 3.2).

The equilibrium mechanical energy release rate, $\mathcal{G}_0$, was found to decrease with water concentration, corresponding to a reduction in the solid-fluid in-

terfacial energy (see Figure 2.7). Within the experimental error, no systematic change in the fitting parameters α and ΔF^* was detected with changing water concentration. This implies that the physical mechanism responsible for crack propagation in calcite is not dependent on the water concentration.

As pointed out by Maugis [59], no particular chemical reaction with the strained bonds at the crack tip is necessary to explain subcritical fracture propagation near $\mathcal{G}_0$. The stress corrosion mechanism for glasses is well established, but in the case of mica it has been argued that the sharpness of the crack makes direct access of environmental species to the strained bonds at the crack tip unlikely. In this case, the most probable rate limited process in region I may be activated interfacial diffusion, which would still yield the functional dependence of Equation (3.8) [58]. More experimental work would be needed in order to resolve whether calcite is more comparable with glass or mica, or whether crack propagation in calcite is controlled by some other, as yet unknown mechanism.

Chapter 4

Effects of stress generation in pores during weathering

In Figure 1.4, three possible effect of stress generation due to crystal growth in pores were presented: Replacement, microcrack propagation and large scale build-up of elastic strain energy. This list is not meant to be extensive. Also, since weathering takes place at low temperatures and confining stresses, plastic deformation and viscous relaxation have been disregarded. This may be an oversimplification in some cases, such as for calcite which behaves plastically even at room temperature (see Paper III). In this chapter the chosen three examples are discussed in more detail.

4.1 Replacement

A very common feature in weathering profiles is the isovolumetric, shape preserving replacement of one mineral by another [107–110]. The shape preservation during replacement is thought to arise due to a stress mediated coupling between the dissolution rate of one mineral and the growth rate of the other mineral. Since this important mechano-chemical coupling has been extensively researched it has not been a focus of the present study, but since it belongs in this context a brief outline of the replacement mechanism is described below.

Imagine a mineral A separated from mineral B by a thin fluid film (Figure 4.1). The fluid film is supersaturated with respect to mineral A and saturated with respect to mineral B, which is soluble under these conditions. The film is assumed to be connected to a larger reservoir so that the concentration of species A and B remains constant. Mineral A is growing due to the supersaturation and, in doing so, the separation between A and B becomes

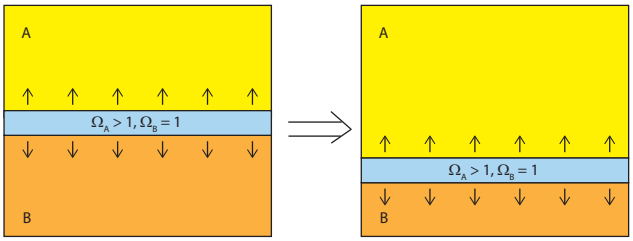

Figure 4.1: Mineral A separated from mineral B by a thin liquid film (blue), which is supersaturated with respect to A and saturated with respect to B. The thickness of the film is greatly exaggerated for clarity. The growth of A results in a normal stress exerted on the interface between A and B which causes B to dissolve. With time, mineral B is replaced by mineral A with no change in volume.

smaller. The decrease in film thickness sets up a disjoining pressure in the fluid film which is equivalent to a normal stress exerted on the surfaces of A and B. This increases the equilibrium concentration of B, causing B to dissolve increasingly faster with increasing decreasing surface separation. At some point, the rate of growth of A (which decreases with increasing normal stress) equals the growth rate of B and the system self-adjusts at a steady state normal stress, the magnitude of which depends on the kinetic constants and specific volumes of A and B as well as the value of Ω_A, but is always smaller than σ_c [111].

Since in this model all of the work exerted by the growing crystal A goes into dissolution of B, the result is isovolumetric replacement of mineral B by A.

As is often the case (and is also illustrated by Paper II), continuum models do not reflect all of the details of the process. When a replacement front is moving into mineral B from all free surfaces, so that there is no obvious connection between the interface between A and B and some larger liquid reservoir, one would expect the liquid film to become saturated with respect to both minerals causing the reaction to stop, since solid state diffusion for most minerals is negligibly slow under weathering conditions. Experimental studies [112–114] have revealed that replacement processes are, in fact, always associated with porosity generation in the replacing mineral. This allows for sustained transport to the interface between A and B through a percolating

network of solution filled pores or fractures. The evolution of this porosity is probably related to local crystal growth kinetics [115].

4.2 Microcrack propagation

If a crystal is growing in a pore with insoluble pore walls, stresses may become large enough to enlarge the pore by fracture propagation. The magnitude of stress required for crack propagation depends on the pore geometry and can be characterized by the mechanical energy release rate $\mathcal{G}$ which is analytically defined for a range of idealized geometries (see Chapter 3).

Microcrack propagation may lead to a variety of weathering morphologies depending on the boundary conditions. Microcracking near the surface of the rock leads to granular disintegration and flaking, which is often observed in experiments on salt crystallization in rocks [116]. A spectacular result of localized granular disintegration is the formation of tafoni structures (Figure 1.2c) [117].

The formation of veins due to crystal growth and propagation of cracks at a fixed energy release rate or stress value has been analyzed by Fletcher and Merino [111], and subcritical crack growth due to ice growth in a temperature gradient, coupled to water transport through a partially frozen matrix, was modelled by Walder and Hallet [118].

4.2.1 Thesis results: Coupling subcritical crack propagation and stress generation due to crystallization

One may envisage a number of geometries in which fractures are propagated directly by the stress generated due to crystal growth in a pore. Two possible geometries are shown in Figure 4.2. The top panel shows radial cracks propagating from a circular pore. These cracks form due to the tangential component of stress which is present in a hole subject to a uniform internal pressure [119]. The bottom panel shows a penny-shaped crack which is pushed open by a crystal growing in its aperture.

While the first geometry might be more intuitively appealing, the second geometry was chosen for the model presented in Paper IV. The reason is that analytical expressions relating the fracture opening and radius to the crystal radius and stress makes it possible to obtain direct relations for the feedback from crack propagation to normal stress and therefore crystal growth rate through the change in crack compliance.

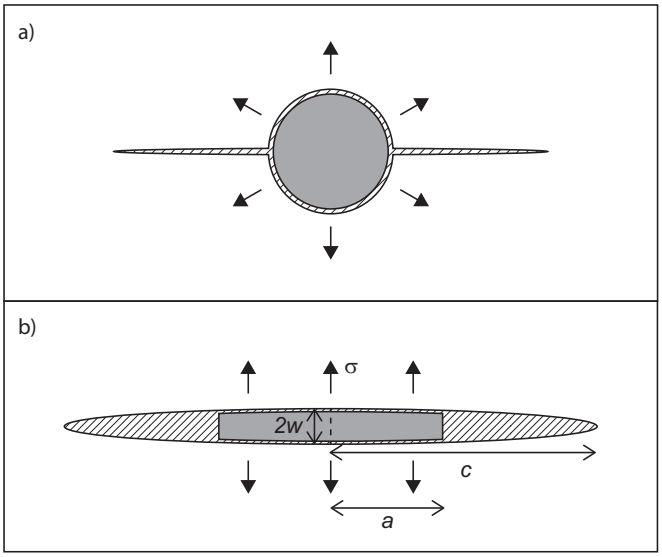

Figure 4.2: Crack propagation due to growth of a crystal (grey) in pore filled with a supersaturated solution (hatched). a) Radial cracks growing from a circular pore. b) Crystal growing in the aperture of a penny-shaped crack with radius c and maximum opening $2w$. The crystal is located in the center of the crack and has radius a and thickness $2w$ which matches the aperture of the crack (the fluid film thickness is assumed to be negligible). The growing crystal exerts a normal stress σ on the crack walls.

Some results for a stationary crack have already been presented in Chapter 2. It turns out that two dimensionless parameters, one which relates crack growth kinetics to crystal growth kinetics and another which characterizes the degree of supersaturation, controls the evolution of fractures. In particular, there is a crossover from dynamic cracking (where the energy release rate $\mathcal{G}$ increases sharply with increasing crack length) to subcritical cracking (where $\mathcal{G}$ is locked at a value close to $\mathcal{G}_0$ for long times) which is given by the two dimensionless parameters. This crossover is illustrated in Figure 4.3.

4.3 Build-up of elastic strain energy and macroscopic expansion

If the solubility of neighbouring minerals is too low for replacement to take place, and the geometry of the pore is such that the threshold for crack propagation is not reached, then crystals may continue to grow in pores until the maximum crystallization stress σ_c is exerted on all pore walls. When crystals exert an isotropic stress in a large number of pores in a homogeneous rock, the result is a bulk volume increase analogous to thermal expansion. If the rock is confined in some directions, the result of the expansion is a build-up of elastic strain energy which may become large enough to propagate large scale fractures.

Spheroidal weathering (Figure 4.4), which is a striking weathering morphology found in many lithologies and in a wide range of geographical settings, is an example of a pattern formed by fractures propagated due to expansion during weathering. This is the prevalent explanation for this pattern [10, 120–123], although alternative hypotheses have been proposed including inherent stress patterns in the rock [124, 125] and chemical processes with no mechanical component [126, 127].

The origin of the bulk expansion resulting in elastic strain and fractures may vary for different lithologies, and it is difficult to identify the exact stress generating reaction by petrological examination of the weathered rock. Buss *et al.* [128] found that the first weathering reaction to take place in a spheroidally weathered quartz diorite in Puerto Rico was an oxidation of biotite which caused an expansion in d(001) from 10.0Å to 10.5Å, which is probably sufficient to produce the observed fractures. In an andesite of relatively high initial porosity, Jamtveit *et al.* [in prep.] found that precipitation of iron oxides in pores from a supersaturated solution was the most probable stress generating mechanism.

The strain ϵ resulting from a mean isotropic stress σ_c in a large number

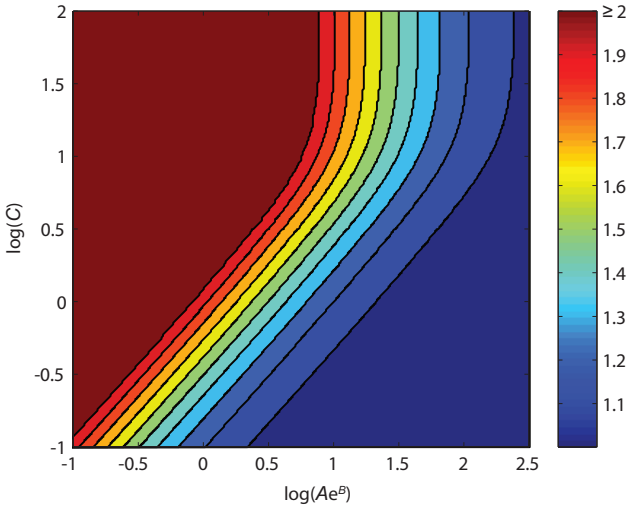

Figure 4.3: The relative value of the mechanical energy release rate, $\mathcal{G}/\mathcal{G}_0$, which is reached in fractures after long times as a function of the dimensionless parameters Ae^B (which relates crack kinetics and crystal growth kinetics) and C (describing the level of supersaturation). The range of parameters has been chosen to illustrate the crossover in behaviour. If $\mathcal{G}/\mathcal{G}_0 > 2$, then the crack is accelerating quickly and the system enters the dynamic fracturing regime. $\mathcal{G}/\mathcal{G}_0$ close to one imply that fractures accelerate extremely slowly and that subcritical fracture propagation is dominating. A perfectly constant crack velocity is never reached which means that at long enough times, the system will become unstable. For a full description of the model, see Paper IV.

Figure 4.4: Road section showing a spheroidally weathered dolerite sill in Karoo, South Africa (see also Paper I).

of pores in a rock which is completely saturated with fluid is given by [129]

$$\epsilon = \frac{bS_c\sigma_c}{K}, \tag{4.1}$$

where K is the bulk modulus of the rock, b is the Biot coefficient of the rock ($b = 1 - K/K_S$ where K_S is the bulk modulus of the solid phase of the rock) and S_c is the volume fraction of pores filled with crystals.

With a crystallization front moving from the free surface and into the rock, the rock is free to expand in the direction normal to the free surface, but constrained in the surface parallel direction. Disregarding surface curvature, this confinement gives rise to a surface parallel stress given by [119]

$$\sigma = 3K\epsilon. \tag{4.2}$$

When the elastic energy built up in the outer layer of the rock is sufficiently large, it can produce spalls by driving fractures parallel to the surface. Assuming a uniform surface parallel on a flat surface, the elastic strain energy is large enough to drive surface parallel cracks when the thickness of the layer is given by [130]

$$\Delta h = \frac{2\Gamma E}{\sigma^2}, \tag{4.3}$$

where Δh is the thickness of the layer and Γ is the surface energy of the rock. The effect of surface curvature can also be included [119, 131], but the expressions become more complicated. This model shows how spalling can be produced by in-pore crystallization, and when realistic parameters are used the length scale given by Equation (4.3) agrees well with observed spall thicknesses [Jamtveit *et al.*, in prep.].

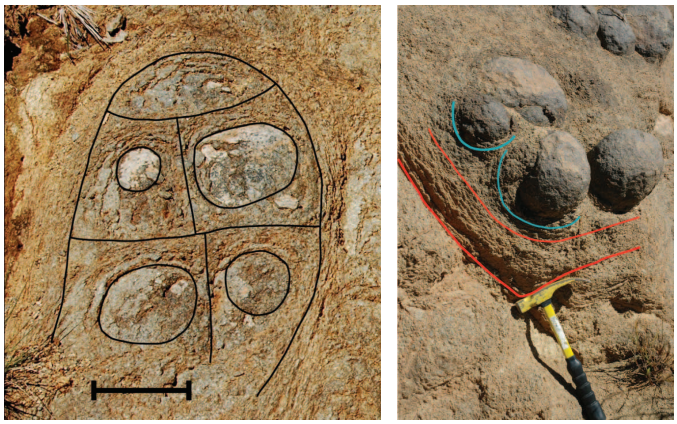

Figure 4.5: Details showing how initially spheroidally weathered blocks have become subdivided into smaller units which have subsequently been rounded by spheroidal weathering.

4.3.1 Thesis results: Hierarchical fracturing

In spheroidal weathering profiles, the rounded blocks or corestones are sometimes observed to become divided into smaller units after some extent of spheroidal weathering of the original block has taken place (Figure 4.5). This is evident from some figures in literature [132, fig. 7],[121, fig. 5],[122, fig. 2], but has not been much discussed, although Sarracino and Prasad [127] suggested that subdivision of corestones during the weathering process was caused by some large scale tectonic event.

In Paper I, we show that the subdivision of corestones during spheroidal weathering can be caused by the same elastic strain energy which is causing the spalling. A conceptual explanation is that expansion of the outer layer of a solid body also generates a tensile stress in the middle of the body [119], which may be sufficient to propagate fractures depending on the geometry. A numerical model demonstrates that subdivision of an initially intact solid due can result from an expansive reaction (Figure 4.6).

The subdivision process can be viewed as a hierarchical process where domains get progressively subdivided with new fractures forming at normal angles to preexisting fractures. The effect of this domain divining process is to accelerate large scale weathering rates since more surface area and more efficient fluid pathways are created through fracturing.

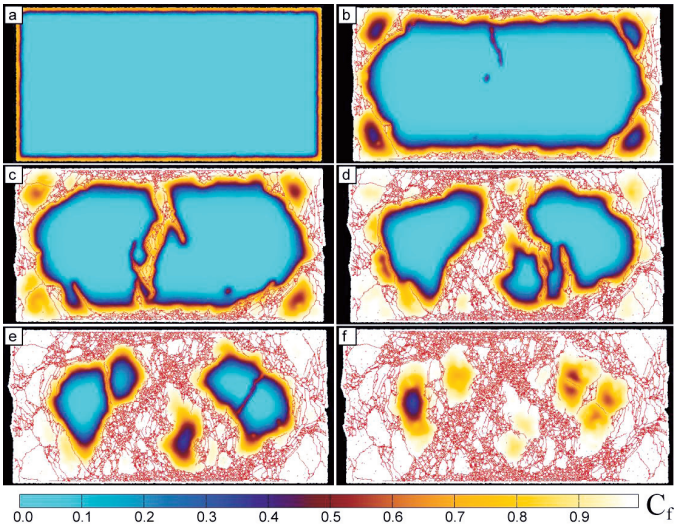

Figure 4.6: Result of a numerical simulation where an initially intact rectangular block reacts with water and expands along the outside. Fracturing causes the block to become progressively subdivided and rounded. The color scale shows the local extent of reaction.

Chapter 5

Summary and outlook

The principal agent in rock weathering is water, and it is the manifestations of the properties of water at different scales which unify the topics adressed in this thesis.

On the large scale, water acts as a transport medium for chemical species. As water penetrates into unweathered rock it allows reactions to take place through dissolution of unstable minerals and precipitation of more stable minerals. The weathering front is an open system where species can be supplied and removed through the aqueous phase.

During spheroidal weathering and the associated hierarchical fracturing of rock, weathering is accelerated due to fracturing because the fractures that open enables faster water transport, and also because more unreacted rock surface area becomes exposed to water. This coupling between mechanical and chemical processes during weathering has been explored in Paper I, where it was shown that stresses generated during weathering can cause fracturing on a larger scale than what was previously recognized. This may have significant implications for the rate of advancement of the weathering front.

On the small scale, stresses are generated in pores when crystals precipitate from a thin film of water at a grain contact. The presence of water at this contact is determined by the long range forces which act between surfaces separated by a thin liquid film. An alternative way of explaining the presence of a thin film of water which transmits a normal stress between two surfaces is to consider the effect of water on the surface energy of the solids. If the sum of the solid-liquid interfacial energies is higher than the energy of the dry solid-solid contact, it may be energetically favourable for the system to sustain a liquid film at an elevated pressure. The complex dynamics of the interface between a growing crystal and a confining wall is illustrated by the experiments presented in Paper II. Contrary to what has been assumed,

there is no tendency for the loaded crystal face to approach a steady state where it is in smooth contact with the confining surface.

If water is present in the aperture of a fracture, the energy of the fracture surfaces are lower than they would have been if the fracture had opened up in vacuum. Since fracture propagation requires the applied mechanical energy to be higher than the energy of the two newly created surfaces, it may require less energy to open a water filled crack than one which is empty. The effect of water on fracture propagation can also be explained in terms of surface forces. The crack tip in brittle materials is thought to be very sharp and to approach molecular dimensions near the tip. If a film of water is present in the crack aperture, then in the region near the crack tip, where the crack opening is very small, long range forces will be acting between the fracture surfaces. When these forces are repulsive, their effect is to increase the effective stress at the crack tip and thus to lower the applied mechanical energy required for crack propagation. The effect of water on the surface energy and crack propagation in calcite is described in Paper III, which shows that increasing the water concentration leads to a monotonic decrease in surface energy of calcite.

Fracture propagation and stress generation due to crystal growth, which are two of the principal processes responsible for damage in rocks during weathering, are thus linked by the physical properties of thin liquid films. They are also both time dependent processes, and coupled through their effect on and response to the stress field around pores and fractures. The model presented in Paper IV shows that the coupling of fracture kinetics and crystallization kinetics may control how fractures evolve when they are driven by crystallization stresses.

During the work of this thesis, some questions have been answered, and many new questions have been raised.

The mechanisms responsible for subcritical crack growth in calcite, and in many other geological materials, are still not known. As any thermally activated process is expected to produce the same type of crack velocity curves, identifying the exact physical or chemical mechanisms would require carefully planned experiments in a range of chemical environment. Theoretical considerations and simulations may also help to understand the relative importance of surface forces and crack-tip reactions such as stress corrosion and dissolution.

The generation of stresses during crystal growth has been explained theoretically by considering the equilibrium between the bulk solution at hydrostatic pressure and the solid subject to a normal stress. In reality, the liquid in intimate contact with the stressed crystal surface is not at hydrostatic pressure. The effect of the disjoining pressure on the chemical potential of

the dissolved material in the thin film has not been fully worked out. This is also the case for the effect of moving a surface on the surface forces transmitted through thin liquid films, something which may be important both for growing crystals and for propagating fractures.

When diffusion takes place under the influence of external forces, it may in some instances result in ions being transported in the direction of greater ion concentration. This may be the case when large pressure gradients are present, such as when the disjoining pressure is localized at areas of contact. It is not known what effect this may have on transport and growth of crystals under normal stress, and on transport of reactive species to the crack tip.

In order to advance the understanding of the process by which crystals perform mechanical work on their surroundings through growth, a more thorough theoretical treatment of the process, including the effects of surface forces, ion diffusion and the nucleation and propagation of steps on a faceted crystal. In situ observations of the evolution of the loaded interface would also be valuable.

In porous materials, transport has large scale effects on whether damage takes place, and on the resulting weathering morphologies (see Figure 5.1). Upscaling from the pore scale to the scale of rock samples requires an understanding of transport processes and how they couple to the kinetics of crystal growth and fracture propagation.

The large scale degradation of rock does not take place by isolated fractures but rather by the interplay between a large number of microfractures. The analysis presented in this thesis on the propagation of a single fracture due to crystal growth can be extended to consider the interactions between fractures and the evolution of fracture populations through time, which may provide useful insight on how rocks are broken due to crystallization stresses.

It is not yet known to what extent biological agents such as plant roots and fungal hyphae actively cause fracture propagation in rocks. The work in this thesis has highlighted the intimate connection between the crack tip chemistry and the stress required to propagate a crack. Since the chemical environment near a root tip is most certainly affected by the plant, it may be relevant to consider whether biological agents are able to cause fracture propagation through excerting a pressure while affecting the crack tip chemistry in order to lower the pressure required for crack growth. This sort of analysis may advance the current understanding of biological weathering.

Figure 5.1: This rock art on Angkor Wat has been damaged due to salt crystallization. The white substance on the surface of the rock is so-called efflorescence, where salts have crystallized on the outside of the rock. Crystallization is more damaging if it takes place in pores within the rock, so-called subflorescence, and this has resulted in fracturing and scaling. Whether efflorescence or subflorescence takes place is largely controlled by transport processes.

Bibliography

[1] S.P. Anderson, J. Blum, S.L. Brantley, O. Chadwick, J. Chorover, L. A. Derry, J. I. Drever, J. G. Hering, J. W. Kirchner, L. R. Kump, D.l Richter, and A. F. White. Proposed initiative would study Earth's weathering engine. *EOS, Transactions, American Geophysical Union*, 85(28):265–272, 2004.

[2] Y. Godderis, Y. Donnadieu, M. Tombozafy, and C. Dessert. Shield effect on continental weathering: Implication for climatic evolution of the Earth at the geological timescale. *Geoderma*, 145:439–448, 2008.

[3] V. G. Nordberg and A. V. Turkington. Weathering geomorphology: Theoretical and methodological themes. *Physical Geography*, 25(5):418–437, 2004.

[4] E. Jagoutz. Salt-induced rock fragmentation on Mars: The role of salt in the weathering of Martian rocks. *Advances in Space Research - Series S*, 38.

[5] M. A. Chan, W. A. Yonkee, D. I. Netoff, W. M. Seiler, and R. L. Ford. Polygonal cracks in bedrock on Earth and Mars: Implications for weathering. *Icarus*, 194:65–71, 2008.

[6] E. Hoffland, T. W. Kuyper, H. Wallander, C. Plassard, A. A. Gurbushina, K. Haselwandter, S. Holmstr´om, R. Landeweert, U. S. Lundstr´om, A. Rosling, R. Sen, M. S. Smiths, P. A. W. van Hess, and N. van Breemen. The role of fungi in weathering. *Frontiers in Ecology and the Environment*, 2(5):258–264, 2004.

[7] A. O. Adeyemi and G. M. Gadd. Fungal degradation of calcium-, lead- and silicon-bearing minerals. *BioMetals*, 18:269–281, 2005.

[8] Y. Wang, Y. Wang, and E. Merino. Dynamic weathering model: Constrints required by coupled dissolution and pseudomorphic replacement. *Geochimica et Cosmochimica Acta*, 59(8):1559–1570, 1995.

[9] S. L. Brantley, J. Bandstra, J. Moore, and A. F. White. Modelling chemical depletion profiles in regolith. *Geoderma*, 145:494–504, 2008.

[10] R. C. Fletcher, H.L. Buss, and S. L. Brantley. A spheroidal weathering model coupling porewater chemistry to soil thickness during steady-state denundation. *Earth and Planetary Science Letters*, 244:444–457, 2006.

[11] M. I. Lebedeva, R. C. Fletcher, V. N. Balashov, and S. L. Brantley. A reactive diffusion model describing transformation of bedrock to saprolite. *Chemical Geology*, 244(3-4):624–645, 2007.

[12] M.I. Lebedeva, R.C. Fletcher, and S.L. Brantley. A mathematical model for steady-state regolith production at constant erosion rate. *Earth Surface Processes and Landforms*, 35:508–524, 2010.

[13] A. F. White, T. D. Bullen, M. S. Schulz, A. E. Blum, T. G. Huntington, and N. E. Peters. Differential rates of feldspar weathering in granitic regoliths. *Geochimica et Cosmochimica Acta*, 65(6):847–869, 2001.

[14] G. E. Hilley, C. P. Chamberlain, S. Moon, S. Porder, and S. D. Willett. Competition between erosion and reaction kinetics in controlling silicate-weathering rates. *Earth and Planetary Science Letters*, 293:191–199, 2010.

[15] A. F. White. Determining mineral weathering rates based on solid and solute weathering gradients and velocities: application to biotite weathering in saprolites. *Chemical Geology*, 190:69–89, 2002.

[16] S. L. Brantley A. F. White. The effect of time on the weathering of silicate minerals: why do weathering rates differ in the laboratory and field? *Chemical Geology*, 202:479–506, 2003.

[17] P. B. Sak, D. M. Fisher, T. W. Gardner, K. Murphy, and S. L. Brantley. Rates of weathering rind formation on Costa Rican basalt. *Geochimica et Cosmochimica Acta*, 68(7):1453–1472, 2004.

[18] G. D. Hoke and D.L. Turcotte. Weathering and damage. *Journal of Geophysical Research - Solid Earth*, 107(B10):2210, 2002.

[19] S.-E. Lauritzen. Karst as a weathering skin phenomenon: Is there a simple, scale-independent model for karstification? In *14th International Congress of Speleology*, pages O–63, Athens-Kalamos, 2005.

[20] C. S. Riebe, J. W. Kirchner, and R. C. Finkel. Long-term rates of chemical weathering and physical erosion from cosmogenic nuclides and geochemical mass balance. *Geochimica et Cosmochimica Acta*, 67(22):4411–4427, 2003.

[21] A. Dosseto, S. P. Turner, and J. Chappell. The evolution of weathering profiles through time: New insights from uranium-series isotopes. *Earth and Planetary Science Letters*, 274(3-4):359–371, 2008.

[22] L. Ma, F. Chabaux, E. Pelt, E. Blaes, L. X. Jin, and S. Brantley. Regolith production rates calculated with uranium-series isotopes at Susquehanna/Shale Hills Critical Zone Observatory. *Earth and Planetary Science Letters*, 297(1-2):211–225, 2010.

[23] S. Taber. Frost heaving. *Journal of Geology*, 37(5):428–461, 1929.

[24] S. Taber. The mechanics of frost heaving. *Journal of Geology*, 38(4):303–317, 1930.

[25] R. R. Gilpin. A model for the prediction of ice lensing and frost heave in soils. *Water Resources Research*, 16(5):918–930, 1980.

[26] G. W. Scherer. Crystallization in pores. *Cement and Concrete Research*, 29(8):1347–1358, 1999.

[27] O. Coussy. Poromechanics of freezing materials. *Journal of the Mechanics and Physics of Solids*, 53(8):1689–1718, 2005.

[28] J. G. Dash, A. W. Rempel, and J. S. Wettlaufer. The physics of premelted ice and its geophysical consequences. *Reviews of Modern Physics*, 78(3):695–741, 2006.

[29] J. B. Murton, R. Peterson, and J.-C. Ozouf. Bedrock fracture by ice segregation in cold regions. *Science*, 314(5802):1127–1129, 2006.

[30] K. Hall. Evidence for freeze-thaw events and their implications for rock weathering in northern Canada: II. The temperature at which water freezes in rock. *Earth Surface Processes and Landforms*, 32(2):249–259, 2007.

[31] J. Lavalle. Recherche sur la formation des cristaux la temprature ordinaire. *Comptes Rendus de l'Academie des Sciences*, 36:49–495, 1853.

[32] G. F. Becker and A. L. Day. The linear force of growing crystals. *Proceedings of the Washington Academy of Sciences*, 8:283–288, 1905.

[33] S. Taber. The growth of crystals under external pressure. *American Journal of Science*, 41:532–556, 1916.

[34] C. W. Correns. Growth and dissolution of crystals under linear pressure. *Discussions of the Faraday Society*, 5:267–271, 1949.

[35] R. J. Flatt, M. Steiger, and G. W. Scherer. A commented translation of the paper by C.W. Correns and W. Steinborn on crystallization pressure. *Environmental Geology*, 52(2):221–237, 2007.

[36] J. W. Gibbs. On the equilibrium of heterogeneous substances. *Transactions of the Connecticut Academy*, 3:108–248, 1876.

[37] M. S. Paterson. Nonhydrostatic thermodynamics and its geologic applications. *Reviews of Geophysics*, 11(2):355–389, 1973.

[38] M. Steiger. Crystal growth in porous materials - II: Influence of crystal size on the crystallization pressure. *Journal of Crystal Growth*, 282(3-4):470–481, 2005.

[39] L.A. Rijniers, H.P. Huinink, and K. Kopinga. Experimental evidence of crystallization pressure inside porous media. *Physical Review Letters*, 94(075503), 2005.

[40] M. Steiger. Crystal growth in porous materials–I: The crystallization pressure of large crystals. *Journal of Crystal Growth*, 282(3-4):455–469, 2005.

[41] P.-G. de Gennes, F. Brochard-Wyart, and D. Quéré. *Capillarity and wetting phenomena: drops, bubbles, pearls, waves*. Springer, New York, 2003.

[42] J. Israelachvili. *Intermolecular and surface forces*. Academic Press, London, 1992.

[43] B. Derjaguin and L. Landau. Theory of the stability of strongly charged lyophobic sols and of the adhesion of strongly charged particles in solutions of electrolytes. *Progress in Surface Science*, 43(1-4):30–59, 1941.

[44] E.J.W. Verwey and J.Th.G. Overbeek. *Theory of the stability of lyophobic colloids*. Elsevier, Amsterdam, 1948.

[45] J. N. Israelachvili and G. E. Adams. Measurement of forces between 2 mica surfaces in aqueous-electrolyte solutions in range 0-100 nm. *Journal of the Chemical Society-Faraday Transactions I*, 74:975–1001, 1978.

[46] N. Alcantar, J. Israelachvili, and J. Boles. Forces and ionic transport between mica surfaces: implications for pressure solution. *Geochimica et Cosmochimica Acta*, 67(7):1289–1304, 2003.

[47] A. Anzalone, J. Boles, G. Greene, K. Young, J. Israelachvili, and N. Alcantar. Confined fluids and their role in pressure solution. *Chemical Geology*, 230(3-4):220–231, 2006.

[48] A. Hamilton, V. Koutsos, and C. Hall. Direct measurement of salt-mineral repulsion using atomic force microscopy. *Chemical Communications*, 46(29):5235–5237, 2010.

[49] R. M. Pashley. Dlvo and hydration forces between mica surfaces in li^+,na^+,k^+,and cs^+ electrolyte-solutions - a correlation of double-layer and hydration forces with surface cation-exchange properties. *Journal of Colloid and Interface Science*, 83(2):531–546, 1981.

[50] R. M. Pashley and J. N. Israelachvili. Molecular layering of water in thin-films between mica surfaces and its relation to hydration forces. *Journal of Colloid and Interface Science*, 101(2):511–523, 1984.

[51] P. K. Weyl. Pressure solution and the force of crystallization - a phenomenological theory. *Journal of Geophysical Research*, 64(11):2001–2025, 1959.

[52] D. K. Dysthe, Y. Podladchikov, F. Renard, J. Feder, and B. Jamtveit. Universal scaling in transient creep. *Physical Review Letters*, 89(24):246102–1 – 246102–4, 2002.

[53] F. Renard, D. Bernard, X. Thibault, and E. Boller. Synchotron 3d microthomography of halite aggregates during experimental pressure solution creep and evolution of the permeability. *Geophysical Research Letters*, 31(L07607):1–4, 2004.

[54] J. P. Gratier, R. Guiguet, F. Renard, L. Jenatton, and D. Bernard. A pressure solution creep law for quartz from indentation experiments. *Journal of Geophysical Research-Solid Earth*, 114, 2009.

[55] N. H. de Leeuw and S. C. Parker. Atomistic simulation of the effect of molecular adsorption of water on the surface structure and energies of calcite surfaces. *J. Chem. Soc., Faraday Trans.*, 93(3):467–475, 1997.

[56] A. A. Griffith. The phenomena of rupture and flow in solids. *Philosophical Transactions of the Royal Society of London, Series A*, 221:163–198, 1921.

[57] C.E. Inglis. Stresses in a plate due to the presence of cracks and sharp corners. *Proc. Inst. Naval Architects*, 55:219, 1913.

[58] B. Lawn. *Fracture of brittle solids*. Cambridge University Press, second edition, 1993.

[59] D. Maugis. Review: Subcritical crack growth, surface energy, fracture toughness, stick-slip and embrittlement. *Journal of Materials Science*, 20:3041–3073, 1985.

[60] J. W. Obreimoff. The splitting strength of mica. *Proceedings of the Royal Society of London. Series A*, 127(805):290–297, 1930.

[61] E. Orowan. The fatigue of glass under stress. *Nature*, 154(3906):341–343, 1944.

[62] J. R. Rice. Thermodynamics of quasi-static growth of Griffith cracks. *Journal of the Mechanics and Physics of Solids*, 26(2):61–78, 1978.

[63] E. Sharon and J. Fineberg. Confirming the continuum theory of dynamic brittle fracture for fast cracks. *Nature*, 397(6717):333–335, 1999.

[64] B.V Deryagin and M.S. Metsik. Role of electrical forces in the process of splitting mica along cleavage planes. *Soviet Physics: Solid State*, 1:1393–1399, 1960.

[65] K.-T. Wan, S. Lathabai, and B. R. Lawn. Crack velocity functions and thresholds in brittle solids. *Journal of the European Ceramic Society*, 6:259–268, 1990.

[66] R.J. Charles. Static fatigue of glass. I. *Journal of Applied Physics*, 29(11):1549–1553, 1958.

[67] S. M Wiederhorn. Influence of water vapor on crack propagation in soda-lime glass. *Journal of the American Ceramic Society*, 50(8):407–414, 1967.

[68] S. M. Wiederhorn and L. H. Bolz. Stress corrosion and static fatigue of glass. *Journal of the American Ceramic Society*, 53(10):543–548, 1970.

[69] S. M. Wiederhorn, S. W. Freiman, E. R. Fuller, and C. J. Simmons. Effects of water and other dielectrics on crack-growth. *Journal of Materials Science*, 17(12):3460–3478, 1982.

[70] T. I. Suratwala and R. A. Steele. Anomalous temperature dependence of sub-critical crack growth in silica glass. *Journal of Non-Crystalline Solids*, 316(1):174–182, 2003.

[71] S. Etter, F. Despetis, and P. Etienne. Sub-critical crack growth in some phosphate glasses. *Journal of Non-Crystalline Solids*, 354(2-9):580–586, 2008.

[72] R. J. Martin. Time-dependent crack growth in quartz and its application to the creep of rocks. *Journal of Geophysical Research*, 77(8):1406–1419, 1972.

[73] R. J. Martin and W. B. Durham. Mechanisms of crack growth in quartz. *Journal of Geophysical Research*, 80(35):4837–4844, 1975.

[74] B. K. Atkinson. A fracture mechanics study of subcritical tensile cracking of quartz in wet environments. *Pure and Applied Geophysics*, 117:1011–1024, 1979.

[75] B. K. Atkinson and P. G. Meredith. Stress corrosion cracking of quartz: a note on the influence of chemical environment. *Tectonophysics*, 77:T1–T11, 1981.

[76] P. G. Meredith and B. K. Atkinson. High-temperature tensile crack propagation in quartz: experimental results and application to time-dependent earthquake rupture. *Earthquake Prediction Research*, 1:377–391, 1982.

[77] J. Dunning, B. Douglas, M. Miller, and S. McDonald. The role of the chemical environment in frictional deformation - stress-corrosion cracking and comminution. *Pure and Applied Geophysics*, 143(1-3):151–178, 1994.

[78] T. Reuschle and M. Darot. The alpha-quartz trigonal symmetry revealed by fracture tests. *European Journal of Mineralogy*, 8(4):695–701, 1996.

[79] J.P. Henry, J. Paquet, and J.P. Tancrez. Experimental study of crack propagation in calcite rocks. *International Journal of Rock Mechanics and Mining Sciences and Geomechanics Abstracts*, 14:85–91, 1977.

[80] B. K. Atkinson. Subcritical crack growth in geological materials. *Journal of Geophysical Research*, 89(B6):4077–4114, 1984.

[81] H.-S. Jeong, S.-S. Kang, and Y. Obara. Influence of surrounding environments and strain rates on the strength of rocks subjected to uniaxial compression. *International Journal of Rock Mechanics and Mining Sciences*, 44:321–331, 2007.

[82] Y. Nara and K. Kaneko. Study of subcritical crack growth in andesite using the double torsion test. *International Journal of Rock Mechanics and Mining Sciences*, 42(4):521–530, 2005.

[83] Y. Nara and K. Kaneko. Sub-critical crack growth in anisotropic rock. *International Journal of Rock Mechanics and Mining Sciences*, 43(3):437–453, 2006.

[84] J. Chevalier, C. Fantozzi, and G. Olagnon. Subcritical crack propagation in 3Y-TZP ceramics: Static and cyclic fatigue. *Journal of the American Ceramic Society*, 82(11):3129–3138, 1999.

[85] R.J. Charles. Static fatigue of glass. II. *Journal of Applied Physics*, 29(11):1554–1560, 1958.

[86] C. Kocer and R. E. Collins. Measurement of very slow crack growth in glass. *Journal of the American Ceramic Society*, 84(11):2585–2593, 2001.

[87] C. Olagnon, J. Chevalier, and V. Pauchard. Global description of crack propagation in ceramics. *Journal of the European Ceramic Society*, 26(15):3051–3059, 2006.

[88] T. A. Michalske and S. W. Freiman. A molecular interpretation of stress corrosion in silica. *Nature*, 295(5849):511–512, 1982.

[89] T.A. Michalske and B. C. Bunker. A chemical kinetics model of glass fracture. *Journal of the American Ceramics Society*, 76(10):2613–2618, 1993.

[90] J.-P. Guin, T. Fett, and S. M. Wiederhorn. Crack-tip structure in soda-lime-silicate glass. *Journal of the American Ceramic Society*, 88(3):652–659, 2005.

[91] M. Ciccotti. Stress-corrosion mechanisms in silicate glasses. *Journal of Physics D: Applied Physics*, 42:214006, 2009.

[92] P. M. Dove. Geochemical control on the kinetics of quartz fracture at subcritical tensile stress. *Journal of Geophysical Research - Solid Earth*, 100(B11):22349–22359, 1995.

[93] C. J. Simmons and S. W. Freiman. Effect of corrosion processes on subcritical crack growth in glass. *Journal of the American Ceramic Society*, 64(11):683–686, 1981.

[94] G.S. White and D. C. Greenspan S. W. Freiman. Corrosion and crack growth in 33% Na_2O-67% SiO_2 and 33% Li_2O-67% SiO_2 glasses. *Journal of the American Ceramic Society*, 69(1):38–44, 1986.

[95] B. Lawn. Chemical processes in crack propagation: kinetic fracture. In *Fracture of brittle solids*. Cambridge University Press, second edition, 1993.

[96] J.-P. Guin and S. M. Wiederhorn. Crack growth threshold in soda lime silicate glass: role of hold-time. *Journal of Non-Crystalline Solids*, 316(1):12–20, 2003.

[97] F. Célarié, S. Prades, D. Bonamy, L. Ferrero, E. Bouchaud, C. Guillot, and C. Marlière. Glass breaks like metal, but at the nanometer scale. *Physical Review Letters*, 90(7):075504, 2003.

[98] J. Guin and S. Wiederhorn. Surfaces formed by subcritical crack growth in silicate glasses. *International Journal of Fracture*, 140(1):15–26, 2006.

[99] D. Bonamy, S. Prades, C.L. Roundtree, L. Ponson, D. Dalmas, E. Bouchaud, K. Ravi-Chandar, and C. Guillot. Nanoscale damage during fracture in silica glass. *International Journal of Fracture*, 140:3–14, 2006.

[100] T. Fett, G. Rizzi, D. Creek, S. Wagner, J. P. Guin, J. M. López-Cepero, and S. M. Wiederhorn. Finite element analysis of a crack tip in silicate glass: No evidence for a plastic zone. *Physical Review B (Condensed Matter and Materials Physics)*, 77(17):174110–9, 2008.

[101] S. M. Widerhorn and E. R. Fuller. Effect of surface forces on subcritical crack growth in glass. *Journal of the American Ceramic Society*, 72(2):248–251, 1989.

[102] M. Seto, M. Utagawa, and X. T. Feng. Subcritical crack growth in rock - effect of chemical additives and in situ observations using scanning electron microscope. *Ninth International Congress on Rock Mechanics, Vols 1 and 2*, pages 1015–1018, 1999.

[103] J.D. Dunning and W.L. Huf. The effect of aqueous chemical environments on crack and hydraulic fracture propagation and morphologies. *Journal of Geophysical Research*, 88(B8):6491–6499, 1983.

[104] J.D. Dunning, D. Petrovski, J. Schuyler, and A. Owens. The effect of aqueous chemical environments on crack propagation in quartz. *Journal of Geophysical Research*, 89(B6):411–4123, 1984.

[105] K.-T. Wan, N. Aimard, S. Lathabai, R. G. Horn, and B. R. Lawn. Interfacial energy states of moisture-exposed cracks in mica. *Journal of Materials Research*, 5(1):172–182, 1990.

[106] S. M. Widerhorn, E. R. Fuller, and R. Thomson. Micromechanics of crack growth in ceramics and glasses in corrosive environments. *Metal Science*, August-September:450–458, 1980.

[107] R. G. Maliva and R. Siever. Diagenetic replacement controlled by force of crystallization. *Geology*, 16(8):688–691, 1988.

[108] T. Dewers and P. Ortoleva. Force of crystallization during the growth of siliceous concretions. *Geology*, 18(3):204–207, 1990.

[109] D. Nahon and E. Merino. Pseudomorphic replacement in tropical weathering: Evidence, geochemical consequences, and kinetic-rheological origin. *American Journal of Science*, 297(April):393–417, 1997.

[110] E. Merino and T. Dewers. Implications of replacement for reaction-transport modeling. *Journal of Hydrology*, 209:137–146, 1998.

[111] R. C. Fletcher and E. Merino. Mineral growth in rocks: Kinetic-rheological models of replacement, vein formation, and syntectonic crystallization. *Geochimica et Cosmochimica Acta*, 65(21):3733–3748, 2001.

[112] A. Putnis. Mineral replacement reactions: from macroscopic observations to microscopic mechanisms. *Mineralogical Magazina*, 66(5):689–708, 2002.

[113] C. V. Putnis, K. Tsukamoto, and Y. Nishimura. Direct observations of pseudomorphism: compositional and textural evolution at a fluid-solid interface. *American Mineralogist*, 90:1909–1912, 2005.

[114] C. V. Putnis, T. Geisler, P. Schmid-Beurmann, T. Stephan, and C. Giampaolo. An experimental study of the replacement of leucite by analcime. *American Mineralogist*, 92:19–26, 2007.

[115] C. Raufaste, B. Jamtveit, T. John, P. Meakin, and D.K. Dysthe. The mechanism of porosity formation during solvent-mediated phase transformations. *Proceedings of the Royal Society A*, In Press, 2010.

[116] M. Angeli, R. Hebert, B. Menendez, C. David, and J. P. Bigas. Influence of temperature and salt concentration on the salt weathering of a sedimentary stone with sodium sulphate. *Engineering Geology*, 115(3-4):193–199, 2010.

[117] C. Rodriguez-Navarro, E. Doehne, and E. Sebastian. Origins of honeycomb weathering: the role of salts and wind. *Geological Society of America Bulletin*, 111(8):1250–1255, 1999.

[118] J. Walder and B. Hallet. A theoretical-model of the fracture of rock during freezing. *Geological Society of America Bulletin*, 96(3):336–346, 1985.

[119] S.P. Timoshenko and J.N. Goodier. *Theory of Elasticity*. McGraw-Hill, Singapore, 1970.

[120] James D. Dana. *Manual of Geology*. American Book Company, 4th edition, 1896.

[121] E. Blackwelder. Exfoliation as a phase of rock weathering. *Journal of Geology*, 33:625–635, 1925.

[122] C.D. Ollier. Causes of spheroidal weathering. *Earth-Science Reviews*, 7:127–141, 1971.

[123] R. L. Folk and E. B. Patton. Buttressed expansion of granite and development of grus in Central Texas. *Zeitschrift für Geomorphologie*, 26(1):17–32, 1982.

[124] J. Jocelyn. Stress patterns and spheroidal weathering. *Nature, Physical Sciences*, 240(November):39–40, 1972.

[125] M.I. Prudêncio, M.A. Sequeira Braga, H. Paquet, J. C. Waerenborgh, L.C.J. Pereira, and M.A. Gouveia. Clay mineral assemblages in weathered basalt profiles from Central and Southern Portugal: climatic significance. *Catena*, 49:77–89, 2002.

[126] T. A. Dodge. An example of exfoliation caused by chemical weathering. *Journal of Geology*, 55(1):38–42, 1947.

[127] R. Sarracino and G. Prasad. Investigation of spheroidal weathering and twinning. *GeoJournal*, 19(1):77–83, 1989.

[128] H. L. Buss, P. B. Sak, S. M. Webb, and S. L. Brantley. Weathering of the Rio Blanco quartz diorite, Luquillo Mountains, Puerto Rico: Coupling oxidation, dissolution, and fracturing. *Geochimica et Cosmochimica Acta*, 72:4488–4507, 2008.

[129] R. M. Espinosa-Marzal and G. W. Scherer. Advances in understanding damage by salt crystallization. *Accounts of Chemical Research*, 43(6):897–905, 2010.

[130] J.W. Hutchinson and Z. Suo. Mixed mode cracking in layered materials. *Advances in Applied Mechanics*, 29:63–191, 1992.

[131] J. W. Hutchinson. Delamination of compressed films on curved substrates. *Journal of the Mechanics and Physics of Solids*, 49(9):1847–1864, 2001.

[132] E.B.A. Bisdom. The role of micro-crack systems in the spheroidal weathering of an intrusive granite in Galicia (NW Spain). *Geologie en Mijnbouw*, 46:333–340, 1967.

Scientific Papers

Paper I

Controls on rock weathering rates by reaction-induced hierarchical fracturing
Anja Røyne, Bjørn Jamtveit and Anders Malthe-Sørenssen (2008)
Earth and Planetary Science Letters, **275**, 364-369

Paper II

Growth rims and interface structure of a crystal face growing from solution while exerting a force of crystallization

Anja Røyne and Dag Kristian Dysthe

to be submitted

Paper III

Experimental investigation of surface energy and subcritical crack growth in calcite

Anja Røyne, Jan Bisschop and Dag Kristian Dysthe (2011)
Journal of Geophysical Research - Solid Earth, **116**, B04204

JOURNAL OF GEOPHYSICAL RESEARCH, VOL. 116, B04204, doi:10.1029/2010JB008033, 2011

Experimental investigation of surface energy and subcritical crack growth in calcite

Anja Røyne,[1] Jan Bisschop,[2] and Dag Kristian Dysthe[1]

Received 1 October 2010; revised 15 December 2010; accepted 10 January 2011; published 9 April 2011.

[1] Subcritical cracking behavior and surface energies are important factors in geological processes, as they control time-dependent brittle processes and the long-term stability of rocks. In this paper, we present experimental data on subcritical cracking in single calcite crystals exposed to glycol-water mixtures with varying water content. We find upper bounds for the surface energy of calcite that decrease with increasing water concentration and that are systematically lower than values obtained from molecular dynamics simulations. The relation of surface energy to water concentration can explain water weakening in chalks. The rate of subcritical crack growth in calcite is well described by a reaction rate model. The effect of increasing water on crack velocity is to lower the threshold energy release rate required for crack propagation. The slope of the crack velocity curve remains unaffected, something which strongly suggests that the mechanism for subcritical cracking in calcite does not depend on the water concentration.

Citation: Røyne, A., J. Bisschop, and D. K. Dysthe (2011), Experimental investigation of surface energy and subcritical crack growth in calcite, *J. Geophys. Res.*, *116*, B04204, doi:10.1029/2010JB008033.

1. Introduction

[2] Subcritical crack growth, refers to the phenomenon of slow crack propagation in brittle materials at stresses below the nominal failure stress [*Lawn*, 1993; *Olagnon et al.*, 2006]. This phenomenon in of importance in the Earth's crust, where water and other active species are present and displacements and stresses are small. Subcritical cracking is argued to be the main mechanism of brittle creep of rocks [*Heap et al.*, 2009; *Scholz*, 2002], and to control the time to failure at constant stress. Subcritical crack growth has thus been used as the underlying mechanism in models of slow earthquakes and aftershocks of major earthquakes [*Helmstetter and Shaw*, 2009].

[3] Calcitic rocks are abundant in many hydrocarbon bearing environments and other settings where reactive fluid transport is important. Faulting and fracturing of carbonate reservoirs have major implications for hydrocarbon fluid pathways [*Agosta et al.*, 2007] and carbonates host many active seismic fault zones [*Miller et al.*, 2004]. Experimental studies show that subcritical cracking plays an important role during the compaction of carbonate sediments [*Croizé et al.*, 2010]. The physical processes controlling subcritical cracking in calcite are still, however, poorly known. Experiments on single calcite crystals [*Dunning et al.*, 1994] have shown a nontrivial dependency on pH and ionic concentrations, while studies on calcitic rocks [*Henry et al.*, 1977; *Atkinson*, 1984] have indicated that these rocks display a complex behavior, different to quartz bearing rocks and glasses. Various mechanisms including dissolution and microplasticity have been proposed to explain subcritical crack growth in calcite [*Atkinson*, 1984]. Unlike many other rocks, calcitic rocks display both plastic and brittle behavior at low stresses and temperature [*Turner et al.*, 1954; *Fredrich and Evans*, 1989; *Schubnel et al.*, 2006], and we therefore expect the fracture behavior of calcite to be more complex than the more commonly studied minerals such as mica and quartz.

[4] Chalk, a highly porous rock composed almost entirely of calcite, has been extensively studied due to its importance as an oil and gas producing reservoir rock. The mechanical strength of water saturated chalk is significantly lower than that of dry or oil saturated chalk. This so-called water weakening effect has been the subject of extensive study, but the underlying mechanism is still not fully understood. *Risnes et al.* [2005] showed that the strength of chalk decreases systematically with water content when saturated with water-glycol mixtures. Glycol is fully miscible with water, and its effect on chalk strength is similar to that of oil. Mixtures of water and glycol therefore allow for a systematic study of the effect of water concentration. *Risnes et al.* [2005] concluded that the water weakening effect is caused by the adhesion properties of water on the calcite surfaces.

[5] Brittle fracture propagation is controlled by the Griffith equilibrium condition, which can be stated as

$$\mathcal{G}_0 - 2\gamma_s^e = 0,$$

where $\mathcal{G}$ is the mechanical energy release rate with $\mathcal{G}_0$ corresponding particularly to the lower limit of crack propagation and γ_s^e is the surface energy of the solid in contact with a given chemical environment. The presence of a chemically

[1]Physics of Geological Processes, University of Oslo, Oslo, Norway.
[2]Institute for Building Materials, ETH Hönggerberg, Zurich, Switzerland.

0148-0227/11/2010JB008033

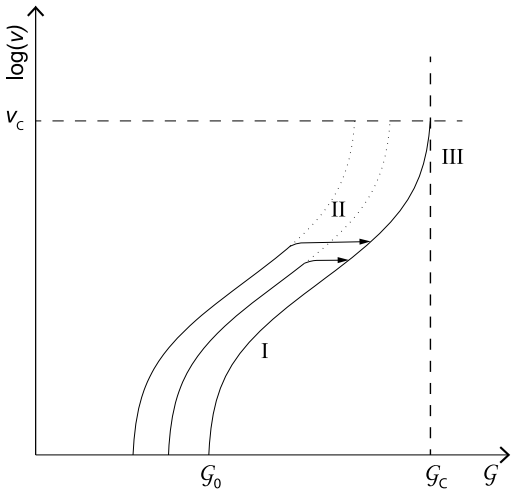

Figure 1. Schematic diagram of subcritical crack propagation [after *Maugis*, 1985]. The curve to the right corresponds to propagation in vacuum. The physical interpretation of regions I, II, and III is given in section 1.

active environment lowers the value of $\mathcal{G}_0$ and as a result the value of v increases for a given value of $\mathcal{G}$ (Figure 1). Measured crack velocity curves $v(\mathcal{G})$ can generally be described by three regions of behavior. In region I, at low $\mathcal{G}$, crack propagation is controlled by reaction kinetics. When transport of active species to the crack tip becomes rate limiting, the system enters region II. The slope of $v(\mathcal{G})$ is typically much lower than in region I. Region III behavior takes place close to the critical energy release rate $\mathcal{G}_c$, where v is a very strong function of $\mathcal{G}$.

[6] Subcritical crack propagation in region I (Figure 1) can be understood as a thermally activated process characterized by forward and backward energy barriers which are functions of $\mathcal{G} - 2\gamma_s^e$ [*Vanel et al.*, 2009], and reaction rate theory gives the following relation for crack velocity v [*Wan et al.*, 1990a]:

$$v = 2\nu_0 a_0 \exp\left(-\frac{\Delta F}{kT}\right) \sinh\left(\frac{\alpha\left(\mathcal{G} - 2\gamma_s^e\right)}{kT}\right), \qquad (1)$$

where $\nu_0 = kT/h$ is a fundamental lattice vibration frequency, k is the Boltzmann constant, T is temperature, a_0 is some characteristic atomic spacing, ΔF is the quiescent value of the energy barrier, and α is an activation area. Experimental data from mica, sapphire and soda-lime silicate glass have been successfully fitted to this model [*Wan et al.*, 1990a]. The phenomenological reaction rate theory does not specify the nature of the process involved.

[7] Surface energies of mineral-fluid interfaces control the presence of fluids at grain boundaries [*de Gennes*, 2003], create an upper bound for the stresses that can be generated by crystal growth in pores [*Espinosa-Marzal and Scherer*, 2010], and control mineral surface morphologies during growth and dissolution [*de Leeuw and Parker*, 1997]. Progress has been made in direct measurements of surface energies by advanced use of the surface forces apparatus [*Alcantar et al.*, 2003; *Anzalone et al.*, 2006] and recently also with atomic force microscopy [*Hamilton et al.*, 2010], but most results from these methods are obtained on mica because of its atomically smooth surface. Molecular simulation studies have been used to determine the surface energies of calcite [*de Leeuw and Parker*, 1997; *de Leeuw et al.*, 1998; *de Leeuw and Cooper*, 2004; *Wright et al.*, 2001; *Kerisit et al.*, 2003; *Kvamme et al.*, 2009] with greatly varying results. Experimental measurements of the surface energy of calcite have been performed using fast fracture experiments with poor control on the environmental conditions [*Gilman*, 1960; *Santhanam and Gupta*, 1968]; surface energies have also been calculated from precipitation studies [*Donnet et al.*, 2005, 2009]. As both of these methods are associated with large uncertainties, better experimental measurements of the surface energies of calcite are needed in order to test the numerical predictions. Subcritical fracture studies represent a complementary method for direct measurements of the surface energies of brittle materials in a range of chemical environments.

[8] In this paper, we present experimental results on the subcritical growth curves and surface energies of calcite in water-glycol mixtures with a range of water concentrations. The results are used to find upper bounds for the surface energies of calcite in these liquids, and to study the effect of water on the crack propagation velocities.

2. Experimental Setup

2.1. Double Torsion Testing

[9] We used the double torsion method [*Evans*, 1972] in our experiments (Figure 2). In this method, a flat sample with an initial notch or starting crack is loaded as shown in Figure 3. Bending of the sample results in propagation of a

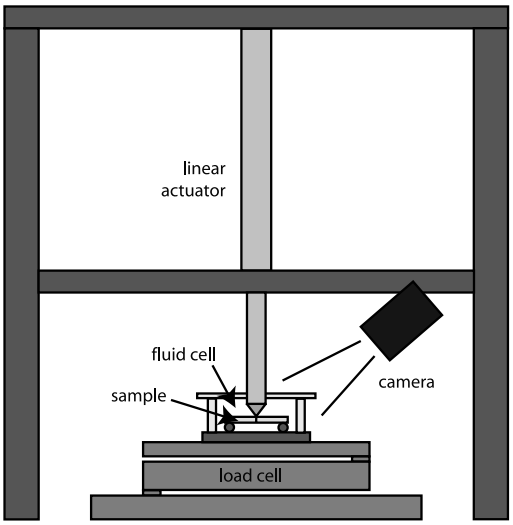

Figure 2. Schematic of the double torsion rig.

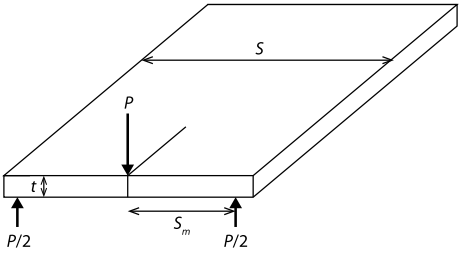

Figure 3. Loading of sample and sample dimensions in the double torsion method.

mode I crack with the highest tensile stress at the bottom side of the sample. This method is well suited for stable crack propagation studies. The energy release rate can be considered to be independent of crack length for the middle portion of the sample, where it can be calculated as [*Shyam and Lara-Curzio*, 2006]

$$\mathcal{G} = \frac{3P^2 S_m^2}{2St^4 G\psi}, \tag{2}$$

where P is the applied load, S_m is half the distance between the supports, S and t are sample width and thickness, $\psi = 1 - 0.6302\tau + 1.20\tau \exp(-\pi/\tau)$ is a geometric correction factor with $\tau = 2t/S$, and G is the shear modulus for calcite (32.8 GPa [*Chen et al.*, 2001]).

[10] Equation (2) is derived from the analytical expression for the sample compliance C [*Shyam and Lara-Curzio*, 2006],

$$C = \frac{\Delta}{P} \approx \frac{3S_m^2}{St^3 G\psi} a, \tag{3}$$

where Δ is the displacement of the loading point. Experimentally, the compliance of the specimen is found to follow the relationship

$$C = \frac{\Delta}{P} = Ba + D, \tag{4}$$

where B and D are scaling constants. The linear dependence of compliance on crack length is only observed in the middle part of the sample, where edge effects are negligible. Reliable measurements can therefore be made for the region of crack lengths where $C(a)$ is linear. The parameter D reflects the compliance of the loading system, while B should be equal to the prefactor in equation (3).

[11] The load relaxation method, where displacement of the loading point Δ is increased quickly and then left constant while the decay of the load P is recorded, is perhaps the most commonly used method in double torsion tests. When the Δ is constant, then the crack velocity $v = \mathrm{d}a/\mathrm{d}t$ can be calculated from the relation

$$v = \frac{-P_i}{P}\left(a_i + \frac{D}{B}\right)\frac{\mathrm{d}P}{\mathrm{d}t}, \tag{5}$$

where P_i and a_i are instantaneous measurements of load and crack length. Ideally, $D/B \ll a$ and can be ignored so that only one crack length measurement is needed. This is particularly useful for nontransparent materials where identification of the crack tip is difficult. In measurements on transparent materials, calculation of v from equation (5) is complementary to direct measurement of crack velocity from the recorded crack length a as a function of time.

2.2. Sample Preparation and Loading

[12] Calcite samples measuring 30 × 10 × 1 mm were cut with the 10 × 30 mm face parallel to the $\{10\bar{1}4\}$ cleavage plane. All of the other faces were cut normal to the $\{10\bar{1}4\}$ plane and thus miscut with respect to the calcite rhomb (Figure 4). The samples were prepared by Photox Optical Systems Ltd. from mined calcite crystals. The 10 × 30 mm surfaces were optically polished. No heterogeneities were visible in the samples when examined between crossed polarizers.

[13] A starting crack was made by scratching near the edge of the sample to produce a slightly rough cleavage crack, 4–5 mm in length. The sample was then loaded in the rig and the crack was forced to propagate to the middle portion of the sample before measurements commenced. In other materials, a guide groove is often necessary to avoid significant crack deflection, and the results can sometimes be affected by the shape of the groove [*Shyam and Lara-Curzio*, 2006], but this was not necessary in our samples due to the strong cleavage of calcite. Crack propagation in other crystallographic directions was not attempted as it is extremely difficult to fracture a single calcite crystal at an angle to a cleavage plane.

[14] All of the experiments were performed at room temperature, which varied with ±0.5°C around 22°C. The water concentration was varied using a mixture of distilled water in ethylene glycol, following the idea from *Risnes et al.* [2005]. The solubility of calcite in pure glycol is 30% lower than in pure water [*Sandengen*, 2006] and both fluid–air surface tension and dielectric constant of glycol are half those of water [*Lide*, 2008]. Several experiments were performed at each mole fraction of 0, 0.1, 0.3, 0.5, 0.7 and 1 of water in glycol. Distilled water was used in all mixtures. The pure glycol may contain as much as 3% water as reported by the manufacturer. Glycol from the same bottle was used for all experiments.

2.3. Experimental Procedure

[15] Due to the small size of the samples (which was limited by the availability of high-quality crystals), the stiffness of the rig D was high compared with the sample compliance B (theoretical value 1.67×10^{-4} N^{-1}, measured values $B = 2.5 \pm 0.4 \times 10^{-4}$ N^{-1} and $D = 1.3 \pm 0.3 \times 10^{-5}$ N^{-1} m). When the sample stiffness is comparable to the stiffness of the loading rig, only a narrow range of crack velocities can be measured in a single load relaxation experiment because P decays less with a than in a stiffer rig. In order to obtain data for as wide a range of stresses as possible, we used a combination of load relaxation measurements (Figure 5) and measurements where the displacement of the loading point was continuously increased. The rate of loading point displacement was increased from 10^{-9} m/s at small crack velocities to 10^{-6} m/s at high velocities. The crack velocities were calculated from the local derivatives of crack length and/or load relaxation

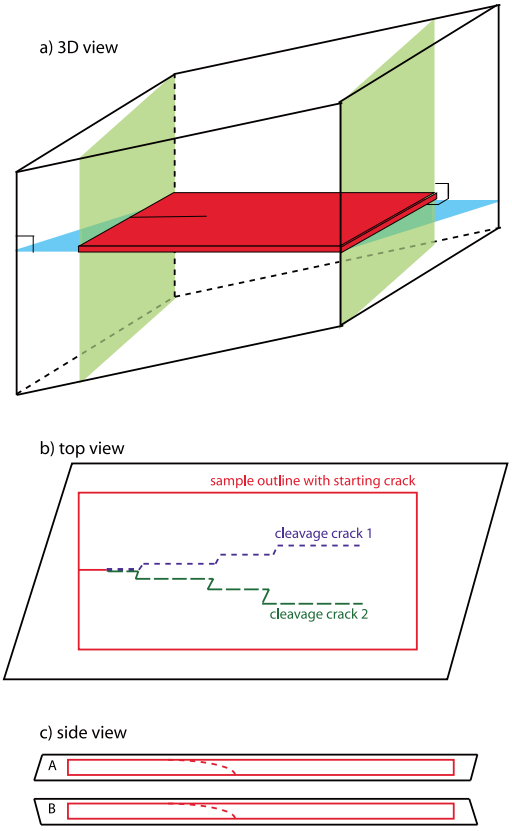

Figure 4. Crystallographic orientation of sample. (a) Sample orientation in relation to the calcite rhomb. (b) Top view of sample, showing the two possible crack directions. The deviation from the center line is greatly exaggerated for clarity. The direction of crack 1 is expected to be more energetically favorable than crack 2. (c) Side view showing the two possible sample orientations. The angle between the cleavage plane and the crack front is larger in A than in B, which may facilitate crack propagation in samples with the B orientation.

measurements (equation (5)) and the energy release rate $\mathcal{G}$ was found from instantaneous load measurements using equation (2).

2.4. Data Acquisition, Processing, and Uncertainty Analysis

[16] The position of the loading point was controlled by a linear actuator (PI M-227.50). The load P was recorded by an Omega load cell with a maximum range of 40 N, and read with a Keithley 2002 multimeter, giving a sensitivity in the load readings of about ±0.001 N. The crack was imaged by adjusting the light source to get maximum reflection from the crack surface, and the crack tip was identified automatically using Matlab software by plotting the light intensity along a profile parallel to the crack and recording where a threshold light intensity was exceeded (Figure 6). Since calcite is a transparent material, crack length measurements are much less problematic than in nontransparent and disordered materials. The linear relationship between compliance and crack length confirms that the crack length detection algorithm is consistent for the entire sample length. Pictures were obtained with a resolution of about 7.5 μm/pixel at a maximum rate of 3 Hz.

[17] After each experiment, the crack surface was examined using a white light interferometer (Wyko NT1100 from Veeco). Scans over the entire crack surface were made with a vertical resolution of about 20 nm. More detailed scans were also made of areas of size 120 × 90 μm with a vertical resolution of about 2 nm. Smaller features, approaching the unit step height of calcite (5 Å) were also visible in these scans, but not quantifiable.

[18] The crack velocities were found by measuring the derivative of crack length with respect to time, and also using equation (5) during load relaxation measurements. The derivatives were estimated by fitting a straight line to a suitable number of data points. This method resulted in an uncertainty in the measured velocity of up to a factor two, depending on the number and quality of pictures or load measurements in the relevant range. The uncertainty in $\mathcal{G}$ calculated from equation (2) is due mainly to the uncertainty in sample thickness t (3%) and shear modulus G (5–10%) and absolute position of the supports S_m (5%) and is estimated to be about 15%. The discrepancy between measured and theoretical sample compliance B may reflect a systematic error leading to a systematic overestimation of $\mathcal{G}$.

[19] The rig was tested for relaxation several times before and between measurements, by leaving it without a sample or with a dummy sample made of stainless steel, at loads higher than those used in the experiments. The relaxation measured in the rig was negligible compared to that measured due to crack growth. In order to test repeatability, we performed some experiments on 76 × 26 × 1 mm glass

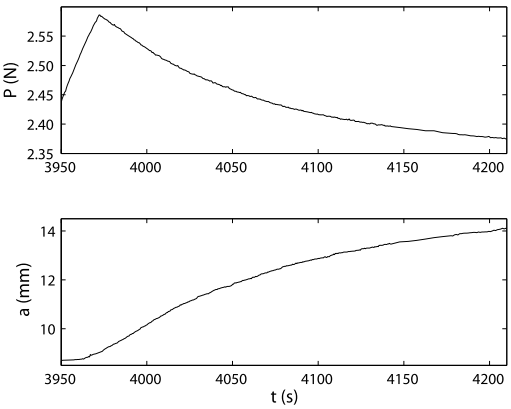

Figure 5. Load P (Newtons) and crack length a (millimeters) measured during one load relaxation experiment. The velocities measured from this plot are the upper portion of measurements shown in blue at $c_w = 0.7$ in Figure 7.

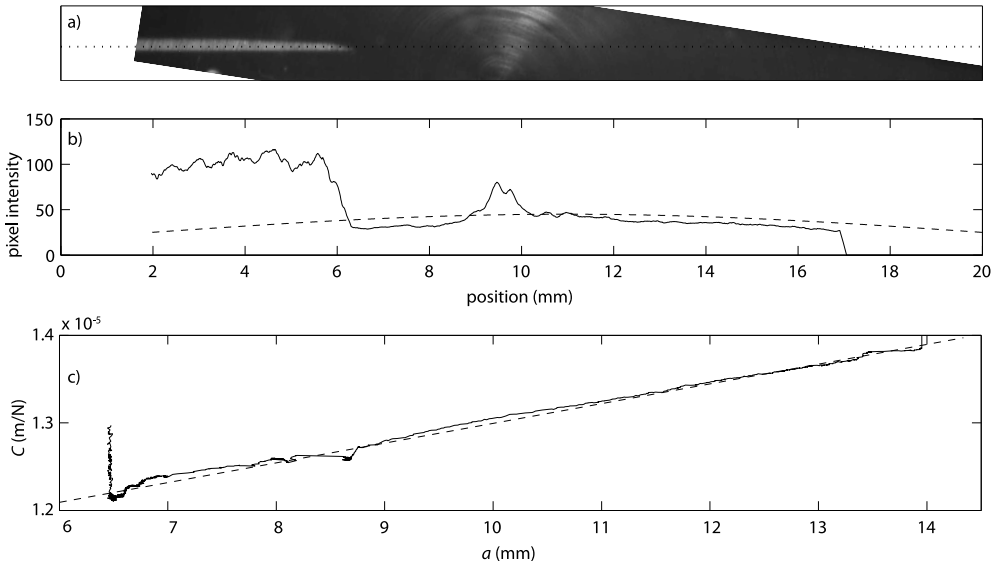

Figure 6. (a) Instantaneous image of the crack tip. The image was rotated to have the crack propagate along the x axis of the picture. (b) Plot along the dotted line in Figure 6a, together with a threshold function (dashed line) which reflects the background intensity. The crack position was taken to be the point where the intensity crossed the threshold curve. When the crack tip was near locations in the cell with high reflections (seen at 10–11 mm in the plot), this had to be corrected manually, and some images were discarded. (c) Compliance curve for this sample. The dashed line shows a linear fit, $C = 2.26 \times 10^{-4}a + 1.07 \times 10^{-5}$ (with a in millimeters).

microscope slides with a very sharp starting crack and without a guide groove, loaded in the same way as the calcite samples. The measured $v(\mathcal{G})$ curves for the glass samples showed a high degree of reproducibility, much more than what we experienced for the calcite samples (see section 4).

3. Results

3.1. Crack Velocities

[20] The measured crack velocity v as a function of energy release rate $\mathcal{G}$ from all our experiments are shown in Figure 7. Measured crack velocities range from 10^{-8} to 10^{-2} m/s. It can be seen that the crack velocity at a given $\mathcal{G}$ is increased by several orders of magnitude when the water concentration is raised.

[21] We find a significant variation in the shapes of the $v(\mathcal{G})$ curves that corresponds to variations in velocity from a factor 2 (pure water) to almost 3 orders of magnitude (pure glycol). This variability is found to be independent of loading method, sample alignment, crack deflection and crack roughness (see Figure 9) and strongly contrast the reproducibility of the tests we made on glass samples. The variation is of similar magnitude for experiments performed both on a single sample and for results for different samples. For any material, a higher energy release rate should always correspond to a higher crack velocity. However, we observe situations in a number of our experiments where v decreases with $\mathcal{G}$ (see section 4).

[22] In the purely brittle regime all of the mechanical energy is converted to crack extension. It follows that the maximum velocity observed at any given $\mathcal{G}$ is the velocity closest to the true brittle $v(\mathcal{G})$ curve, while lower velocities are caused by additional dissipative processes. For each water fraction we have picked a number of maximum velocities (open black symbols in Figure 7) which we take to represent the "brittle $v(\mathcal{G})$ curve" for the respective conditions.

3.2. Surface Energies

[23] Conservative estimates of $\gamma_s^e = \mathcal{G}_0/2$ were made by recording the lowest measured $\mathcal{G}$ at which crack growth was observed, which gives upper bounds for the true values of $\mathcal{G}_0$. With increasing water concentration, we obtained surface energies of 0.32, 0.30, 0.23, 0.12, 0.14 and 0.15 J/m^2 (Table 1 and Figure 8).

3.3. Crack Surface Topography

[24] Figure 9 shows the crack surface topography for one of the experiments ($c_w = 0.5$). The crack surface morphologies are typical for cleavage surfaces, with steps repeating down to the nanometer scale. All of the crack surfaces show steps which are orthogonal to the crack front. This type of step is expected to form on cleavage surfaces due to crack interaction with screw dislocations [*Gilman*, 1959]. The

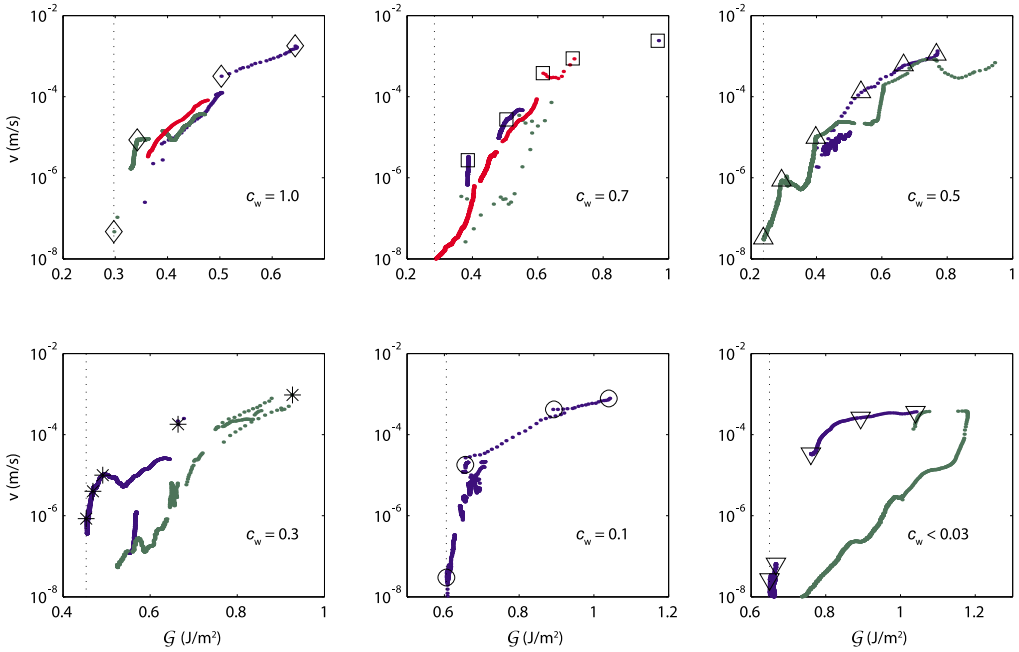

Figure 7. Results from the crack experiments. Each panel corresponds to a different water concentration, c_w. Data points from all experiments are included and are shown in different colors. $\mathcal{G}_0$ is shown as a vertical dotted line. Open black symbols denote high-velocity points that we have extracted and shown in the collapse in Figure 10. Note that the velocity scale is the same for all frames, while the $\mathcal{G}$ scale varies.

ratio of vertical to horizontal displacement is 10^{-4} which means that the direct contribution of fracture steps normal to the fracture direction is negligible. One may also observe in Figure 9 that the surface step direction and step density does not seem to correlate with the crack velocity.

4. Discussion

4.1. Surface Energy of Calcite

[25] The measured surface energy of calcite (Figure 8) decreases with water concentration, and the value of γ_s^e is more than doubled when the water concentration goes from 1 to close to 0. This is consistent with the ratio between the dielectric constants and air/fluid surface tensions of glycol and water [*Lide*, 2008], which are 0.5.

[26] In Figure 8 we have compared our surface energy measurements with the molecular dynamics simulation data of *de Leeuw and Parker* [1997] for surface energies of the calcite cleavage plane at varying degrees of water coverage, from vacuum to one full monolayer at zero Kelvin. Our data and the data of *de Leeuw and Parker* [1997] show similar trends, suggesting that water causes an almost linear decrease in surface energy. Our data extend the already noticed discrepancy between results from experiments and modeling. For wet calcite surfaces, we would have expected experimental results to be higher than the numerical values, because the experimental calcite surfaces always contain steps. The lower experimental values for wet surfaces therefore strongly suggest that there are relaxation effects at water covered calcite surfaces that are not taken into account by current atomistic models. For the dry surfaces, we can explain the lower experimental values by considering that there is always some residual water adsorbed on the calcite surfaces, and in our case "dry" surfaces are covered with glycol, which also lowers the surface energy from the vacuum state.

[27] The trend in our data is consistent with the decrease in hydrostatic yield stress with increasing water activity that was found by *Risnes et al.* [2005] for chalk saturated with water-glycol mixtures. Our findings therefore support Risnes' hypothesis that the principal mechanism causing the water weakening effect is related to decreased cohesion of the chalk grains.

4.2. Crack Velocity Model

[28] Subcritical crack growth in region I (see Figure 1) can be understood as a thermally activated process as described by equation (1). Figure 10 shows a fit of this model to our data. Assuming a characteristic spacing of $a_0 = 5$ Å [*Stipp and Hochella*, 1991], we get good agreement with our data with the parameters for the activation area $\alpha = 2.9 \times 10^{-20}$ m^2 and the quiescent energy barrier $\Delta F = 7.6 \times 10^{-20}$ J.

Table 1. Comparison of Surface Energies γ_s^e of Dry and Fully Hydrated Calcite Surfaces Found Experimentally and Numerically for the $\{10\bar{1}4\}$ Surface as Reported in Literature

Reference	γ_s^e, Dry (J/m^2)	γ_s^e, Wet (J/m^2)
Experimental Results[a]		
This study	0.32	0.15
Donnet et al. [2005]		0.046 ± 0.007
Donnet et al. [2005]		0.135 ± 0.029
Donnet et al. [2009]		0.039–0.164
Gilman [1960]	0.23	
Santhanam and Gupta [1968]	0.347 ± 0.045	
Simulation Results		
de Leeuw and Parker [1997]	0.60	0.30
de Leeuw et al. [1998]	0.59	0.17
de Leeuw and Cooper [2004]	0.59	0.33
Wright et al. [2001]	0.32	0.23
Kerisit et al. [2003]	0.59	0.21
Kvamme et al. [2009]	0.86	0.29

[a]The measurements of *Donnet et al.* [2005] are from precipitation studies, while those of *Gilman* [1960] and *Santhanam and Gupta* [1968] are from fracture experiments.

This can be compared with the results of *Wan et al.* [1990a] for mica, which are $\alpha = 1.5 \times 10^{-19}$ m^2 and $\Delta F = 7.1 \times 10^{-20}$ J with $a_0 = 4.6$ Å. There is no indication of a systematic change of fitting parameters with water concentration. This indicates that a single mechanism, independent of water concentration, controls subcritical crack growth in calcite at the velocities we have studied. The exact physical mechanism controlling subcritical crack growth in calcite cannot be indentified from these measurements. The activation areas correspond to length scales of 1.4 Å for calcite and 3.9 Å for mica, which are both on the order of the atomic spacing. This supports the notion of atomically sharp cleavage cracks in brittle crystals.

[29] Our findings and those of *Dunning et al.* [1994] indicate that the low-velocity plateau described by *Henry et al.* [1977] and *Atkinson* [1984] does not exist in single calcite crystals. If it is a real effect, it must be caused by some property of polycrystalline rocks rather than processes in calcite cleavage. This could be related to processes on the grain boundaries, or to effects related to plasticity in grains which are oriented favorably for twinning.

4.3. Origin of Variable Crack Velocity Data

[30] Our measured $v(\mathcal{G})$ curves (Figure 7) are highly variable, in particular at low c_w and high $\mathcal{G}$. A number of other studies have found subcritical crack growth to be more erratic with decreasing water concentration. For metals, this has been explained by plasticity in the form of local stick-slip [*Briggs et al.*, 1981] while in the case of mica, it has been attributed to surface charge effects [*Deryagin and Metsik*, 1960; *Wan et al.*, 1990b]. In calcite, it has been shown experimentally that twins readily develop at the crack tip at room temperature. This process is reversible up to a certain stress threshold, but it is still a dissipative, nonelastic process [*Bowden and Cooper*, 1962]. It is therefore likely that there are stress-dependent, intermittent, dissipative

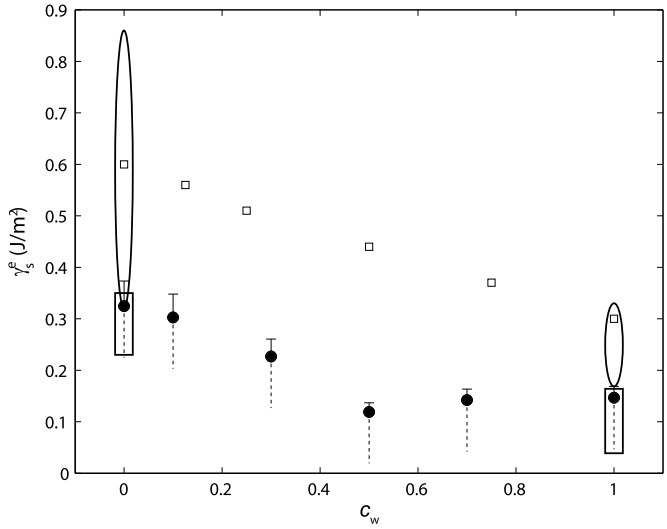

Figure 8. Surface energies γ_s^e of calcite as a function of water concentration (mole fraction or surface cover fraction). Filled circles are estimates from experiments on calcite (this study). The measured γ_s^e are plotted with asymmetric error bars: the upper shows the experimental uncertainty, while the lower is undefined, indicating that our values represent upper bounds. Open squares are surface energies for calcite surfaces with partial coverage of water, calculated by atomistic simulations by *de Leeuw and Parker* [1997]. Ellipses show the range of numerical results from literature for dry and wet calcite surfaces, while rectangles show the range of experimental results from literature (see Table 1).

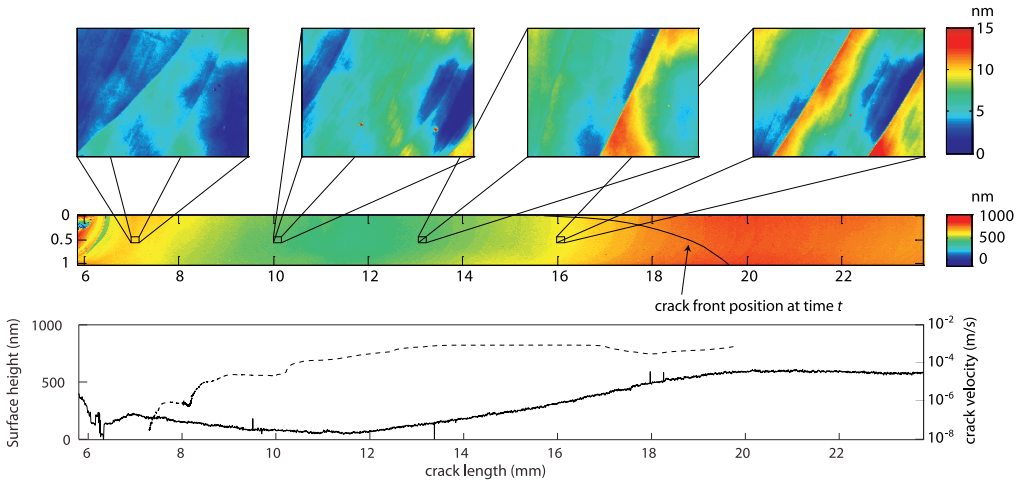

Figure 9. Crack surface topography of one of the 50% water experiments (plotted in green in Figure 7) together with the surface height along the middle of the sample (solid line) and crack velocity (dashed line) as a function of crack length. No correlation was found between the variations in velocity and crack surface topography. Some 120 × 90 μm high-resolution surface images are also included, showing typical cleavage surface steps down to the crystal unit step height.

processes occurring at the crack tip in calcite which do not leave a visible trace on the crack surfaces.

[31] Variations may also be due to effects of crystallographic orientation. On the small scale, some left-right wandering around the cleavage plane is observed (Figure 9), which would result in variation of the ratio of type 1 to type 2 cleavage cracks (see Figure 4). Since type 1 cracks are expected to more energetically favorable, this may have an effect on the observed crack velocity. Slight sample misalignment may cause these effects to become more

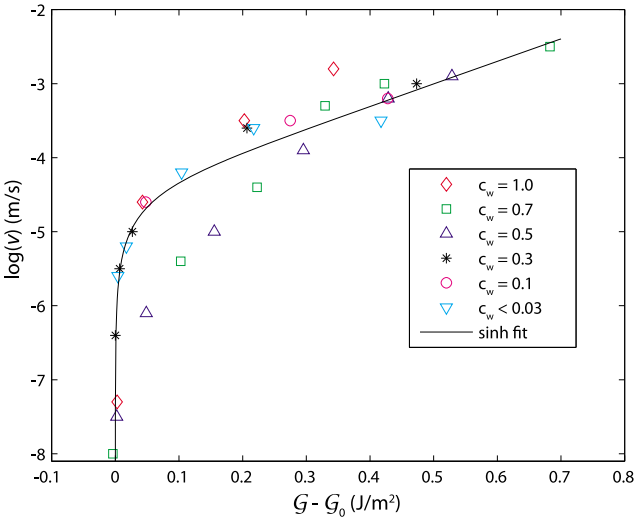

Figure 10. High-velocity points shown in Figure 7, plotted as a function of $\mathcal{G} - \mathcal{G}_0$. The line shows a fit to the model of *Wan et al.* [1990a] (equation (1)) for region I subcritical crack propagation, with fitting parameters $\alpha = 2.9 \times 10^{-20}$ m^2 and $\Delta F = 7.6 \times 10^{-20}$ J.

dominant. More research is needed in order to fully understand the origin of the crack velocity variations.

5. Conclusion

[32] Double torsion experiments on subcritical cracking in calcite represent an alternative method for measuring the effect of chemical environment on the surface energy of calcite. Our results for different water concentrations are consistent with previous experimental results, and are consistently lower than results from numerical simulations. The discrepancy points to relaxation effects that are not properly accounted for in the simulations.

[33] The observed large variations in crack velocity at a given energy release rate may be caused by intermittent plastic processes in calcite, or by some other unidentified process. The highest measured velocities at any given $\mathcal{G}$, which are taken to represent the truly brittle behavior, can be well described using a reaction rate model with parameters similar to those for mica. These findings support the notion of an atomically sharp cleavage crack. There is no indication that the mechanism of subcritical crack growth in calcite is dependent on the water concentration.

[34] Subcritical crack measurements such as those presented here represent an opportunity for measuring the surface energies of different minerals in a wide range of chemical environments. Improved experimental control and higher optical resolution could yield better constrained estimates of $\mathcal{G}_0$. These experimental results would be highly valuable for the validation of numerical simulations. More knowledge on the surface energies of different minerals could also provide us with new insight on how fluids move and reactions take place in a heterogeneous rock.

[35] **Acknowledgments.** We thank Paul Meakin and Francois Renard for helpful comments to the manuscript. Comments made by the two reviewers significantly improved the paper. This study was supported by a Center of Excellence grant from the Norwegian Research Council to the Physics of Geological Processes (PGP) Center.

References

Agosta, F., M. Prasad, and A. Aydin (2007), Physical properties of carbonate fault rocks, Fucino Basin (central Italy): Implications for fault seal in platform carbonates, *Geofluids*, *7*(1), 19–32.

Alcantar, N., J. Israelachvili, and J. Boles (2003), Forces and ionic transport between mica surfaces: Implications for pressure solution, *Geochim. Cosmochim. Acta*, *67*(7), 1289–1304.

Anzalone, A., J. Boles, G. Greene, K. Young, J. Israelachvili, and N. Alcantar (2006), Confined fluids and their role in pressure solution, *Chem. Geol.*, *230*(3–4), 220–231.

Atkinson, B. K. (1984), Subcritical crack growth in geological materials, *J. Geophys. Res.*, *89*(B6), 4077–4114.

Bowden, F. P., and R. E. Cooper (1962), Velocity of twin propagation in crystals, *Nature*, *195*(4846), 1091–1092.

Briggs, A., R. Airey, and B. C. Edwards (1981), A double torsion fracture mechanics and auger electron spectroscopy approach to the study of stress corrosion cracking in low alloy steels, *J. Mater. Sci.*, *16*(1), 125–140.

Chen, C. C., C. C. Lin, L. G. Liu, S. V. Sinogeikin, and J. D. Bass (2001), Elasticity of single-crystal calcite and rhodochrosite by brillouin spectroscopy, *Am. Mineral.*, *86*(11–12), 1525–1529.

Croizé, D., K. Bjørlykke, J. Jahren, and F. Renard (2010), Experimental mechanical and chemical compaction of carbonate sand, *J. Geophys. Res.*, *115*, B11204, doi:10.1029/2010JB007697.

de Gennes, P.-G. (2003), *Capillarity and Wetting Phenomena: Drops, Bubbles, Pearls, Waves*, Springer, New York.

de Leeuw, N. H., and T. G. Cooper (2004), A computer modeling study of the inhibiting effect of organic adsorbates on calcite crystal growth, *Cryst. Growth Des.*, *4*(1), 123–133.

de Leeuw, N. H., and S. C. Parker (1997), Atomistic simulation of the effect of molecular adsorption of water on the surface structure and energies of calcite surfaces, *J. Chem. Soc. Faraday Trans.*, *93*(3), 467–475.

de Leeuw, N. H., S. C. Parker, and K. H. Rao (1998), Modeling the competitive adsorption of methanoic acid on calcite and fluorite surfaces, *Langmuir*, *14*, 5900–5906.

Deryagin, B. V., and M. S. Metsik (1960), Role of electrical forces in the process of splitting mica along cleavage planes, *Sov. Phys. Solid State*, *1*, 1393–1399.

Donnet, M., P. Bowen, N. Jongen, J. Lemaître, and H. Hofmann (2005), Use of seeds to control precipitation of calcium carbonate and determination of seed nature, *Langmuir*, *21*(1), 100–108.

Donnet, M., P. Bowen, and J. Lemaître (2009), A thermodynamic solution model for calcium carbonate: Towards an understanding of multi-equilibria precipitation pathways, *J. Colloid Interface Sci.*, *340*(2), 218–224.

Dunning, J., B. Douglas, M. Miller, and S. McDonald (1994), The role of the chemical environment in frictional deformation: Stress corrosion cracking and comminution, *Pure Appl. Geophys.*, *143*(1–3), 151–178.

Espinosa-Marzal, R. M., and G. W. Scherer (2010), Advances in understanding damage by salt crystallization, *Acc. Chem. Res.*, *43*(6), 897–905.

Evans, A. G. (1972), Method for evaluating time-dependent failure characteristics of brittle materials—and its application to polycrystalline alumina, *J. Mater. Sci.*, *7*(10), 1137–1146.

Fredrich, J. T., and B. Evans (1989), Micromechanics of the brittle to plastic transition in Carrara marble, *J. Geophys. Res.*, *94*(B4), 4129–4145.

Gilman, J. J. (1959), Cleavage, ductility and tenacity in crystals, in *Fracture*, edited by B. L. Averbach et al., pp. 193–222, John Wiley, New York.

Gilman, J. J. (1960), Direct measurement of the surface energies of crystals, *J. Appl. Phys.*, *31*(12), 2208–2218.

Hamilton, A., V. Koutsos, and C. Hall (2010), Direct measurement of salt-mineral repulsion using atomic force microscopy, *Chem. Commun.*, *46*(29), 5235–5237.

Heap, M. J., P. Baud, and P. G. Meredith (2009), Influence of temperature on brittle creep in sandstones, *Geophys. Res. Lett.*, *36*, L19305, doi:10.1029/2009GL039373.

Helmstetter, A., and B. E. Shaw (2009), Afterslip and aftershocks in the rate-and-state friction law, *J. Geophys. Res.*, *114*, B01308, doi:10.1029/2007JB005077.

Henry, J., J. Paquet, and J. Tancrez (1977), Experimental study of crack propagation in calcite rocks, *Int. J. Mech. Min. Sci. Geomech. Abstr.*, *14*, 85–91.

Kerisit, S., S. C. Parker, and J. H. Harding (2003), Atomistic simulation of the dissociative adsorption of water on calcite surfaces, *J. Phys. Chem. B*, *107*(31), 7676–7682.

Kvamme, B., T. Kuznetsova, and D. Uppstad (2009), Modelling excess surface energy in dry and wetted calcite systems, *J. Math. Chem.*, *46*, 756–762.

Lawn, B. (1993), *Fracture of Brittle Solids*, 2nd ed., Cambridge Univ. Press, Cambridge, U. K.

Lide, D. R. (Ed.) (2008), *CRC Handbook of Chemistry and Physics: A Ready-Reference Book of Chemical and Physical Data*, 89th ed., CRC Press, Boca Raton, Fla.

Maugis, D. (1985), Review: Subcritical crack growth, surface energy, fracture toughness, stick-slip and embrittlement, *J. Mater. Sci.*, *20*, 3041–3073.

Miller, S. A., C. Collettini, L. Chiaraluce, M. Cocco, M. Barchi, and B. J. P. Kaus (2004), Aftershocks driven by a high-pressure CO_2 source at depth, *Nature*, *427*(6976), 724–727.

Olagnon, C., J. Chevalier, and V. Pauchard (2006), Global description of crack propagation in ceramics, *J. Eur. Ceram. Soc.*, *26*(15), 3051–3059.

Risnes, R., M. Madland, M. Hole, and N. Kwabiah (2005), Water weakening of chalk - mechanical effects of water-glycol mixtures, *J. Petrol. Sci. Eng.*, *48*, 21–36.

Sandengen, K. (2006), Prediction of mineral scale formation in wet gas condensate pipelines and in MEG (Mono Ethylene Glycol) regeneration plants, Ph.D. thesis, Norw. Univ. of Sci. and Technol., Trondheim, Norway.

Santhanam, A. T., and Y. P. Gupta (1968), Cleavage surface energy of calcite, *Int. J. Mech. Min. Sci. Geomech. Abstr.*, *5*(3), 253–259.

Scholz, C. H. (2002), *The Mechanics of Earthquakes and Faulting*, 2nd ed., Cambridge Univ. Press, Cambridge, U. K.

Schubnel, A., E. Walker, B. D. Thompson, J. Fortin, Y. Gueguen, and R. P. Young (2006), Transient creep, aseismic damage and slow failure in Carrara marble deformed across the brittle-ductile transition, *Geophys. Res. Lett.*, *33*, L17301, doi:10.1029/2006GL026619.

Shyam, A., and E. Lara-Curzio (2006), The double-torsion testing technique for determination of fracture toughness and slow crack growth behavior of materials: A review, *J. Mater. Sci.*, *41*(13), 4093–4104.

Stipp, S. L., and M. F. Hochella (1991), Structure and bonding environments at the calcite surface as observed with X-ray photoelectron spectroscopy (XPS) and low-energy electron-diffraction (LEED), *Geochim. Cosmochim. Acta*, *55*(6), 1723–1736.

Turner, F. J., D. T. Griggs, and H. Heard (1954), Experimental deformation of calcite crystals, *Geol. Soc. Am. Bull.*, *65*(9), 883–934.

Vanel, L., S. Ciliberto, P. P. Cortet, and S. Santucci (2009), Time-dependent rupture and slow crack growth: Elastic and viscoplastic dynamics, *J. Phys. D Appl. Phys.*, *42*, 214007, doi:10.1088/0022-3727/42/21/214007.

Wan, K.-T., S. Lathabai, and B. R. Lawn (1990a), Crack velocity functions and thresholds in brittle solids, *J. Eur. Ceram. Soc.*, *6*, 259–268.

Wan, K.-T., N. Aimard, S. Lathabai, R. G. Horn, and B. R. Lawn (1990b), Interfacial energy states of moisture-exposed cracks in mica, *J. Mater. Res.*, *5*, 172–182.

Wright, K., R. T. Cygan, and B. Slater (2001), Structure of the (10$\bar{1}$4) surfaces of calcite, dolomite and magnesite under wet and dry conditions, *Phys. Chem. Chem. Phys.*, *3*(5), 839–844.

J. Bisschop, Institute for Building Materials, ETH Hönggerberg, HIF E 13.2, Schafmattstr. 6, CH-8093 Zürich, Switzerland. (jbisschop@ethz.ch)

D. K. Dysthe and A. Røyne, Physics of Geological Processes, University of Oslo, PO Box 1048 Blindern, Oslo N-0316, Norway. (d.k.dysthe@fys.uio.no; anja.royne@fys.uio.no)

Paper IV

Subcritical crack propagation driven by crystal growth

Anja Røyne, Paul Meakin, Anders Malthe-Sørenssen, Bjørn Jamtveit and Dag Kristian Dysthe

submitted to PRB

Subcritical crack propagation driven by crystal growth

Anja Røyne,* Anders Malthe-Sørenssen, Bjørn Jamtveit, and Dag Kristian Dysthe
Physics of Geological Processes (PGP), University of Oslo, P.O. Box 1048, 0316 Oslo, Norway

Paul Meakin
Physics of Geological Processes (PGP), University of Oslo, P.O. Box 1048, 0316 Oslo, Norway
Carbon Resource Management Department, Idaho National Laboratory, USA and
Institute for Energy Technology, Kjeller, Norway
(Dated: April 12, 2011)

Crystals that grow in confinement may exert a force on their surroundings and thereby drive crack propagation in rocks and other materials. We describe a model of crystal growth in an idealized crack geometry in which the crystal growth and crack propagation are coupled through the stress in the surrounding bulk solid. Two non-dimensional parameters, which relate the kinetics of crack propagation and crystal growth to the supersaturation of the fluid and the elastic properties of the surrounding material, determine whether dynamic or subcritical crack propagation will take place.

I. INTRODUCTION

Crystallization in pores can generate stresses sufficient to cause damage in a wide range of porous materials, including rocks, masonry, and concrete. It is also believed to be the principal mechanism driving weathering related to freeze-thaw cycles [1, 2] or infiltration of salt-containing fluids [3, 4], and it may also cause vein formation [5, 6] and grain fragmentation in rocks [7].

While a large body of work has focused on damage caused by crystal growth in pores [8], and an equilibrium thermodynamic framework for the bulk deformation that this process may lead to has been established [9], it is still not fully understood how crystal growth controls fracture propagation in the surrounding medium. Subcritical crack growth plays a key role in fracture development when stresses are generated slowly [10, 11], and subcritical crack growth coupled to water transport through a partially frozen rock has proved to be a successful model for fracture propagation during freezing [1].

In this paper, we use an idealized fracture model to analyze the coupling between stress generation by crystal growth from a supersaturated solution and subcritical crack propagation. This provides a basis for understanding the formation of crack networks driven by crystal growth and the associated force of crystallization.

II. THEORETICAL BACKGROUND

A. Stress due to crystal growth

The thermodynamic equilibrium of a non-hydrostatically stressed solid in contact with its solution has been thoroughly established [12–14], although it has not, to date, been firmly demonstrated experimentally [15]. In the absence of stress, the excess chemical potential $\Delta\mu$ driving crystal growth is given by $\Delta\mu = kT\ln\beta$, where k is the Boltzmann constant, T is the temperature and β is the supersaturation defined as the ratio between the ion activity product in solution and the solubility product of the solid. It can be shown that a surface normal stress σ reduces the excess chemical potential to [13]

$$\Delta\mu = kT\ln\beta - \sigma v_0, \tag{1}$$

where v_0 is the specific volume (per particle) of the mineral corresponding to the precipitation reaction used to calculate the supersaturation. Consequently, the equilibrium normal stress σ_c, corresponding to zero crystal growth, is given by [14]

$$\sigma_c = \frac{kT\ln\beta}{v_0}. \tag{2}$$

This approximation is valid for crystal sizes above $\approx 1\mu$m, below which σ_c is lowered by the effect of curvature [16].

In order for a growing crystal to perform mechanical work by displacing a confining wall in the direction of normal load, a liquid film must be present between the crystal face and the confining surface through which ions are supplied to the growing crystal surface [17–19]. The normal stress between the crystal face and the confining wall is transmitted by the disjoining pressure in the liquid film, which increases with decreasing film thickness [20] and becomes significant when the thickness of the film is less than about 10 nm [21]. Disjoining pressures are well described by colloidal theory and have been measured for a range of materials and fluid environments [22].

The growth velocity of a confined crystal face subject to a normal load has not been measured experimentally. However, growth kinetics are known to be rate limiting for the inverse process, pressure solution, for quartz

*anja.royne@fys.uio.no

[23] and if growth kinetics are rate limiting, the supersaturation β will be constant across the confined crystal surface. A good first order approximation is then (using standard crystal kinetic theory [24]) that the rate of crystal growth is proportional to the excess chemical potential. This gives

$$\frac{\mathrm{d}w}{\mathrm{d}t} = Kv_0(\sigma_c - \sigma), \tag{3}$$

where K is a kinetic constant and $\frac{\mathrm{d}w}{\mathrm{d}t}$ is the growth velocity of one face of a crystal of thickness $2w$ when that face is subject to a normal stress σ. It has also been shown [18] that, close to equilibrium, the surface velocity varies linearly with stress for diffusion limited growth. We will therefore assume that the rate of crystal growth is given by equation (3) in our model.

If the stress on the crystal surface is not uniform, then according to equation (3), portions of the surface at which the stress is lower than the mean surface stress will experience a higher growth velocity, while areas where the stress is higher will grow more slowly. As a consequence, the distance to the confining wall and subsequently the surface normal stress will tend to be uniform across the confined crystal surface.

Studies of the influence of mechanical stress on the growth and dissolution rates of crystals have also shown that variation in the growth/dissolution rate is due primarily to the change in free energy of the stressed surface [25]. It follows that, apart from differences due to crystal anisotropy, the kinetic constant K is the same for both the stressed and unstressed crystal faces. The growth rate of the stress free face for a crystal of radius a is then

$$\frac{\mathrm{d}a}{\mathrm{d}t} = Kv_0\sigma_c. \tag{4}$$

B. Subcritical crack growth

The stress field at the tip of a crack may be characterized by the energy release rate $\mathcal{G}$, which is a function of the applied stress, crack length and crack geometry [26]. When $\mathcal{G} = \mathcal{G}_0$, the elastic energy released during incremental crack growth exactly matches the incremental surface energy of the material under the prevailing environmental conditions [11], and the fracture is in thermodynamic equilibrium. If a stress sufficient to make $\mathcal{G}$ exceed a critical value, $\mathcal{G}_c$, is applied sufficiently rapidly to the fracture, the fracture will propagate at a velocity which approaches the Rayleigh wave velocity in the material. If, on the other hand, $\mathcal{G}$ is smaller than $\mathcal{G}_c$ but larger than $\mathcal{G}_0$, much slower subcritical crack growth will take place. Using the theory of thermally activated processes, the crack velocity can be described by the equation

$$\frac{\mathrm{d}c}{\mathrm{d}t} = 2\nu_0 a_0 \exp\left(-\frac{\Delta F}{kT}\right)\sinh\left(\frac{\alpha(\mathcal{G}-\mathcal{G}_0)}{kT}\right), \tag{5}$$

where $\nu_0 = kT/h$ is a characteristic lattice vibration frequency, a_0 is a characteristic atomic spacing, ΔF is the quiescent value of the energy barrier, and α is an activation area [27]. As $\mathcal{G}$ increases, a second regime with a close to constant crack growth velocity is often encountered. Here, the rate of crack growth is limited by the rate of transport of active species to the crack tip. In the third regime, the crack velocity increases sharply as $\mathcal{G} \to \mathcal{G}_c$. Here we consider only the first regime of crack growth, described by equation (5).

Experimental data on subcritical cracking in rocks is most commonly fitted to the empirical Charles' law [10], which expresses the crack velocity as a power of the stress intensity factor. Using this model instead of equation (5) does not qualitatively change our results.

III. THE MODEL

The conceptual model used in this work consists of a crystal growing from a supersaturated solution in the aperture of a fluid-filled penny-shaped crack (Figure 1) of radius c and maximum opening $2w$. The crack is connected to a larger fluid reservoir, so that the supersaturation in the fluid is constant during crystal growth. The crystal is assumed to nucleate in the center of the crack, and to grow in such a manner that the side faces are stress free while there is a uniform normal stress σ on the crystal faces that are separated from the crack walls by a thin fluid film.

When a penny-shaped crack is subject to a radially symmetric stress distribution $\sigma_r(r)$, where r is the radial coordinate, then the stress intensity factor at the crack tip is given by [26]

$$K_I = \frac{2}{\sqrt{\pi c}}\int_0^c \frac{r\sigma(r)}{\sqrt{c^2 - r^2}}\mathrm{d}r. \tag{6}$$

In the model, the stress distribution is given by

$$\sigma_r(r) = \begin{cases} \sigma & 0 \geq r \geq a \\ 0 & r > a \end{cases} \tag{7}$$

which gives

$$K_I = \frac{2\gamma}{\sqrt{\pi}}\sigma\sqrt{c}, \tag{8}$$

where

$$\gamma = 1 - \sqrt{1 - \left(\frac{a}{c}\right)^2}. \tag{9}$$

The wall displacement $w_r(r)$ of a penny-shaped crack subject to the stress distribution described by equation (7) is given by [28]

$$\begin{aligned}\frac{w_r(r)}{c} &= \frac{4}{\pi E'}\sigma\Big(\gamma\sqrt{1-\left(\frac{r}{c}\right)^2} + \\ &\quad \frac{a}{c}\left[\mathbb{E}\left(r/a\right) - \mathbb{E}\left(\arcsin\left(r/c\right), a/c\right)\right]\Big),\end{aligned} \tag{10}$$

where $E' = E/(1-\nu^2)$ under plane strain conditions, $\mathbb{E}(\phi, k)$ is the second elliptical integral and $\mathbb{E}(k)$ is the complete second elliptical integral. Since the rate of opening $\frac{dw_r}{dt}$ during crystal growth and crack extension is smallest in the center of the crack, equation (10) can be solved for the maximum crack opening w where $r = 0$. In this case, $k = 0$ which gives $\mathbb{E}(0) = \frac{\pi}{2}$ and $\mathbb{E}(\phi, 0) = \arcsin(\phi)$. The displacement in the crack center is then given by

$$\frac{w}{c} = \frac{4}{\pi E'}\sigma(\gamma + \psi) \tag{11}$$

with $\psi = (a/c)\left[\pi/2 - \arcsin(a/c)\right]$.

Using the relationship between the energy release rate $\mathcal{G}$ and the stress intensity factor K_I [26],

$$\mathcal{G} = \frac{K_I^2}{E'}, \tag{12}$$

the relationship

$$\mathcal{G} = \frac{\pi E'}{4}\frac{w^2}{c}\left(\frac{\gamma}{\gamma + \psi}\right)^2 \tag{13}$$

can be derived using equations (8) and (11).

For a crack subject to an internal fluid pressure p, the energy release rate is given by

$$\mathcal{G} = \frac{4}{\pi E'}p^2 c. \tag{14}$$

Therefore an equivalent pressure

$$p = \frac{w}{c}\left(\frac{\gamma}{\gamma + \psi}\right), \tag{15}$$

which corresponds to the fluid pressure which would be required to achieve the same value of $\mathcal{G}$ as that observed in the system, can be assigned. Note that $\sigma = p$ when $a = c$.

IV. ANALYSIS

As the crystal nucleates and begins to grow, the energy release rate is initially not large enough for the fracture to propagate. The evolution of stress σ and equivalent pressure p are determined by the crystal growth kinetics and fracture compliance. If the crystal rapidly grows to fill the crack, the increase in $\sigma = p$ if $a = c = c_0$ (where c_0 is the initial crack radius) is given by equation (11) so that

$$\frac{d\sigma}{dt} = \frac{\pi E'}{4c_0}\frac{dw}{dt}.$$

Substituting the expression for $\frac{dw}{dt}$ from equation (3) into this equation gives

$$\frac{d\sigma}{dt} = \frac{\pi E'}{4c_0}\frac{dw}{dt} = \frac{\pi E' K v_0}{4c_0}(\sigma_c - \sigma),$$

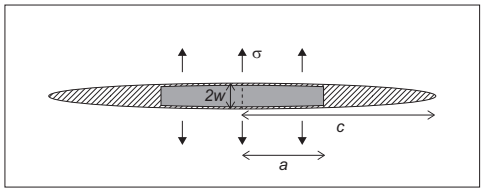

FIG. 1: Conceptual model. A crystal (grey) is growing from a supersaturated solution (hatched) in a penny-shaped crack with radius c and maximum opening $2w$. The crystal is located in the center of the crack and has radius a and thickness $2w$, which matches the aperture of the crack (the fluid film thickness is assumed to be negligible). The growing crystal exerts a normal stress σ on the crack walls, which is transmitted by the disjoining pressure in the confined liquid film.

which can be solved to yield (with $\sigma(0) = 0$)

$$\sigma = \sigma_c\left(1 - e^{-t/t_0}\right), \tag{16}$$

where $t_0 = \frac{4c_0}{\pi E' K v_0}$. This implies that as long as the crack is stationary, the normal stress on the crack walls will approach σ_c; this will happen more slowly if the crystal radius a takes a long time to reach c_0. Often the "crystallization pressure" is simply assumed to be a function of supersaturation. However, equation (16) indicates that this pressure only asymptotically approaches σ_c, at a rate which is determined by t_0.

Crack propagation is initiated when $\mathcal{G}$, given by equation (13), reaches $\mathcal{G}_0$. If $\sigma_c < \sqrt{\frac{\pi E' \mathcal{G}_0}{4c_0}}$, this limit will never be reached and the crack will not grow. The critical crack radius, c_c, is thus given by

$$c_c = \frac{\pi E' \mathcal{G}_0}{4\sigma_c^2}. \tag{17}$$

The ratio $t_c = \frac{4c_c}{\pi E' K v_0}$ provides a natural time scale for the system, and the dimensionless variables $t^* = t/t_c, c^* = c/c_c, w^* = w/c_c, a^* = a/c_c, \sigma^* = \sigma/\sigma_c$ and $p^* = p/\sigma_c$ completely characterize the model. Introducing the dimensionless groups

$$A = \frac{8\nu_0 a_0}{\pi E' K v_0}\exp\left(-\frac{\Delta F}{kT}\right), B = \frac{\alpha \mathcal{G}_0}{kT}, C = \frac{4\sigma_c}{\pi E'},$$

the system is described in dimensionless form by the equations

$$\sigma^* = \frac{1}{C}\frac{w^*}{c^*}\frac{1}{\gamma + \psi}, \tag{18}$$

$$p^* = \frac{1}{C}\frac{w^*}{c^*}\frac{\gamma}{\gamma + \psi}, \tag{19}$$

$$\frac{dc^*}{dt^*} = \begin{cases} 0 & \text{if } c^* p^{*2} \leq 1 \\ A\sinh\left(B(c^* p^{*2} - 1)\right) & \text{if } c^* p^{*2} > 1 \end{cases} \quad (20)$$

$$\frac{dw^*}{dt^*} = C(1 - \sigma^*), \quad (21)$$

$$\frac{da^*}{dt^*} = \begin{cases} C & \text{if } a^* < c^* \\ \frac{dc^*}{dt^*} & \text{if } a^* = c^* \end{cases} \quad (22)$$

Crack propagation due to a filled pore ($a^* = c^*$) is completely described by the parameters A and B, which determine how the crack growth and crystal growth kinetics are related to the elastic moduli of the material. The dimensionless parameter C, which is a function of the supersaturation, only controls crystal growth in the unloaded direction, and therefore determines the maximum crack velocity at which the crystal continues to fill the crack. It also determines how long it takes to build up the initial equivalent pressure p^* in the crack and subsequently the time at which the fracture propagation is initiated.

In a filled pore, the time required for the crack propagation to initiate, $t^* = t_1^*$, can be found by solving the dimensionless form of equation (16) for $c^* \sigma^{*2} = 1$, which gives

$$t_1^* = -c_0^* \ln\left(1 - \sqrt{\frac{1}{c_0^*}}\right). \quad (23)$$

This function has a minimum when $c_0^* \approx 2$. Furthermore, as $c_0^* \to 1$, $t_0^* \to \infty$, because small cracks require an effective pressure very close to σ_c in order for $p^* \sigma^{*2}$ to reach the value of 1, which is required for growth (equation 20). The effect of smaller C is to increase t_1^*. The effect is greater for larger c_0^*, so that the minimum of t_1^* is shifted to lower c_0^*.

V. NUMERICAL RESULTS

The model was investigated by solving the set of equations (18)-(22) numerically for a range of parameters A, B, C and c_0. Figure 2 shows the resulting time evolution of the stress and equivalent pressure in a single crack. Initially, the stress σ^* is higher than the effective pressure $p*$ due to the small area over which the on the crystallization pressure is applied. As the crystal grows unrestricted in the radial direction, the effective pressure increases more rapidly than σ^* because stresses that are applied closer to the crack tip contribute more to the stress intensity factor than stresses applied in the center of the crack (see equation (8)). At point I, the crystal has grown to fill the fracture ($a^* = c^*$), and subsequent crystal growth results in an increase in $p^* = \sigma^*$ as described by equation (16). Crack propagation is initiated at point II, after which p^* and σ^* fall off from

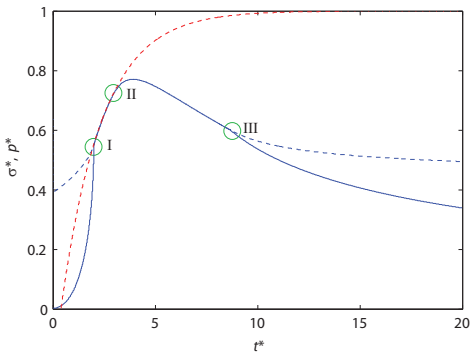

FIG. 2: Time evolution of the crystal stress σ^* (dashed blue line) and effective pressure p^* (solid line) for $A = B = C = 1$ and $c_0^* = 2$. The red dashed line shows the asymptotic increase in stress which is predicted for a stationary, filled crack according to equation (16). The circles show: I. how $\sigma^* = p^*$ increases according to equation (16) when the crystal has grown to fill the crack, so that $a^* = c_0^*$; II. the initiation of crack propagation; and III. the point where $\frac{da^*}{dt^*} < \frac{dc^*}{dt^*}$ so that the crystal no longer fills the crack, and $\sigma^* > p^*$.

the exponential curve and decrease as the effect of increased fracture compliance becomes dominant. After point III has been reached, the velocity of the crack tip is faster than the growth rate of the free crystal face, so that $a^* < c^*$. This increases σ^* and consequently decreases the rate of crystal growth, which makes the rate of crack propagation slower than it would have been if the crack had remained filled.

The time at which fracture propagation is initiated, and whether the crystal grows to fill the crack before it starts to propagate, is determined by the initial crack radius c_0^*, as shown in the upper panel of figure 3.

After the point at which $\frac{d^2 p^*}{dc^{*2}} > 0$, the dimensionless equivalent pressure p^* and the normal stress σ^* do not depend on the initial dimensionless crack radius c_0^*, but are uniquely defined by c^*. This is evident in the lower panel of figure 3. The implication is that after an initial transient, memory of the initial conditions is lost, so that a crack for which $\frac{d^2 p^*}{dc^{*2}} > 0$ could have started out at any $c_0^* < c^*$.

It is reasonable to assume that the subcritical crack growth model (equation (5)) is valid for $c^* p^{*2} \leq 2$. If $c^* p^{*2}$ exceeds a value of 2 within a short time or before the crack has grown appreciably, the system may enter the dynamic crack propagation regime, where inertial effects and dissipative mechanisms not considered in this model may become important. At $c^* p^{*2} = 2$, $\frac{dc^*}{dt^*} \approx Ae^B$. This means that the combination of parameters Ae^B and C should determine whether the crack re-

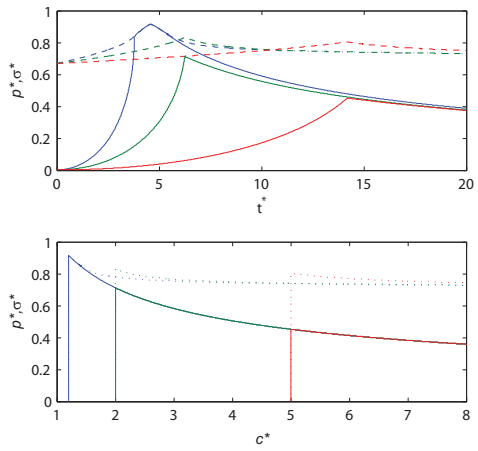

FIG. 3: Evolution of crystal stress σ^* (dashed line) and effective pressure p^* (solid line) as a function of time t^* (upper panel) and crack radius c^* (lower panel) for cracks of initial radius 1.2 (blue), 2 (green) and 5 (red) c_c. In this simulation, $A = 10$, $B = 2$ (so that $Ae^B = 73.9$) and $C = 10^{-0.5}$.

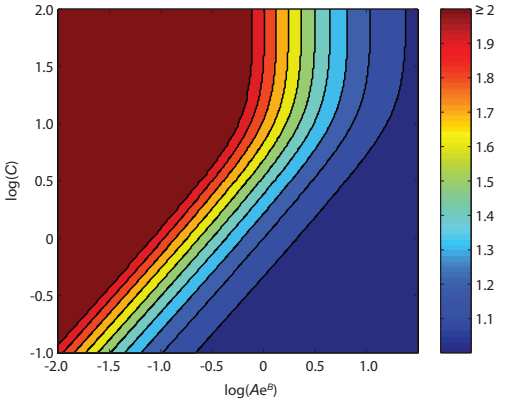

FIG. 4: The value of c^*p^{*2} reached at $c^* = 1000$ as a function of Ae^B and C for $c_0^* = 2$. For $c^*p^{*2} > 2$ the model is out of its range of validity, and the system may enter the dynamic fracture growth regime. The range of parameters are chosen to show the crossover from a power law dependence on C at low Ae^B and C to a regime which is insensitive to C (because C is large enough to maintain $a = c$ at any crack velocity of interest), and the crossover from dynamic to subcritical cracking as Ae^B increases.

mains subcritical.

Figure 4 shows a contour plot of the value of c^*p^{*2} that is reached when $c^* = 1000$ for a range of values of Ae^B and C. The simulations were stopped if $c^*p^{*2} > 2$. The cutoff at $c^* = 1000$ was chosen because very large cracks are expected to interact with other cracks in realistic systems, and we do not include the effects of crack-crack interactions. The interpretation of figure 4 is that blue colors in the plot correspond to more "subcritical" behaviour. If Ae^B is high, crack propagation is sufficiently fast compared with the rate of stress generation due to crystal growth that even if the crystal fills the crack at all times, the system can approach a steady state in which stress generation by crystal growth is almost balanced by crack propagation. For low Ae^B, fast crystal growth and slow crack propagation allows c^*p^{*2} to reach a large value before the stress is relieved by crack propagation, and the system may enter the dynamic fracture regime. The effect of lowering C is to increase the range of Ae^B at which crack propagation is subcritical. This happens because the ratio a^*/c^* becomes smaller as the crack is propagating, so that the effective pressure p^* decreases faster than it would for a filled crack. This has a stabilizing effect on the value of c^*p^{*2} as the crack grows, which allows longer periods of subcritical crack growth (because the fracture acceleration never goes completely to zero, all cracks in this model will become unstable at long enough times).

VI. APPLICATIONS

In nature, there are huge variations in both crystal growth and fracture propagation kinetics. Data available in the scientific literature [6, 27, 29] yield values for Ae^B which span almost 20 orders of magnitude, ranging from 4.2×10^{-5} for gypsum growing in glass, through 3.3 for calcite in glass to 1.1×10^{15} for quartz in mica. Based on Figure 4, we would expect quartz to produce subcritical fractures in mica under all conditions (the model for mica from [27] is only valid for $c^*p^{*2} < 1.2$, but this is irrelevant at such a high value of Ae^B because c^*p^{*2} approaches steady state at a value very close 1). Calcite growing in glass would cause it to break dynamically after some time provided that the supersaturation is high enough. In order for gypsum to produce subcritical fractures in glass, the supersaturation would need to be very low.

It has been shown that statistical properties of fracture networks may be strongly influenced by the degree of subcritical crack propagation [30, 31]. In light of the current results, this would imply that the effect of fracture propagation in rocks due to crystal growth may be highly variable depending on the mineralogy and chemistry of the host rock and growing minerals.

VII. CONCLUSION

To summarize, we have shown that the coupling between crystal growth in a crack and subcritical crack growth has implications for the evolution of fractures when fracture propagation is driven by growing crystals. The dimensionless parameters Ae^B (which relates the crack growth kinetics and the crystal growth kinetics) and C (which characterizes the degree of supersaturation) determine whether cracks will propagate dynamically or subcritically. For a wide range of parameters, subcritical crack growth cannot be ignored, and must be taken into account in models that describe the damage generated due to salt weathering.

Acknowledgements

We thank Raymond C. Fletcher for helpful comments to the manuscript. This study was supported by a Center of Excellence grant from the Norwegian Research Council to the Center for the Physics of Geological Processes (PGP).

[1] J. Walder and B. Hallet, Geological Society of America Bulletin **96**, 336 (1985).
[2] J. B. Murton, R. Peterson, and J.-C. Ozouf, Science **314**, 1127 (2006).
[3] G. W. Scherer, Cement and Concrete Research **34**, 1613 (2004).
[4] C. Rodriguez-Navarro and E. Doehne, Earth Surface Processes and Landforms **24**, 191 (1999).
[5] D. V. Wiltschko and J. W. Morse, Geology **29**, 79 (2001).
[6] R. C. Fletcher and E. Merino, Geochimica et Cosmochimica Acta **65**, 3733 (2001).
[7] E. P. Rothrock, Journal of Geology **33**, 80 (1925).
[8] R. M. Espinosa-Marzal and G. W. Scherer, Accounts of chemical research **43**, 897 (2010).
[9] O. Coussy, Journal of the Mechanics and Physics of Solids **54**, 1517 (2006).
[10] B. K. Atkinson, Journal of Geophysical Research **89**, 4077 (1984).
[11] D. Maugis, Journal of Materials Science **20**, 3041 (1985).
[12] J. W. Gibbs, Transactions of the Connecticut Academy **3**, 108 (1876).
[13] M. S. Paterson, Reviews of Geophysics **11**, 355 (1973).
[14] M. Steiger, Journal of Crystal Growth **282**, 455 (2005).
[15] R. J. Flatt, M. Steiger, and G. W. Scherer, Environmental Geology **52**, 221 (2007).
[16] M. Steiger, Journal of Crystal Growth **282**, 470 (2005).
[17] C. W. Correns, Discussions of the Faraday Society **5**, 267 (1949).
[18] P. K. Weyl, Journal of Geophysical Research **64**, 2001 (1959).
[19] G. W. Scherer, Cement and Concrete Research **29**, 1347 (1999).
[20] R. M. Espinosa-Marzal and G. W. Scherer, in *Limestone in the built environment: Present-day challenges for the preservation of the past.*, edited by B. J. Smith, M. Gomez-Heras, H. A. Viles, and J. Cassar (The Geological Society of London, London, 2010), vol. 331 of *Geological Society, London, Special Publications*, pp. 61–77.
[21] A. Anzalone, J. Boles, G. Greene, K. Young, J. Israelachvili, and N. Alcantar, Chemical Geology **230**, 220 (2006).
[22] J. Israelachvili, *Intermolecular and surface forces* (Academic Press, London, 1992).
[23] R. van Noort, C. J. Spiers, and G. M. Pennock, Journal of Geophysical Research-Solid Earth **113** (2008).
[24] A. Lasaga, *Kinetic theory in the Earth sciences* (Princeton University Press, Princeton, 1998).
[25] J. N. Sherwood and R. I. Ristic, Chemical Engineering Science **56**, 2267 (2001).
[26] B. Lawn, *Fracture of brittle solids* (Cambridge University Press, 1993), 2nd ed.
[27] K.-T. Wan, S. Lathabai, and B. R. Lawn, Journal of the European Ceramic Society **6**, 259 (1990).
[28] T. Fett, International Journal of Fracture **20**, R135 (1982).
[29] D. R. Lide, *CRC handbook of chemistry and physics: a ready-reference book of chemical and physical data* (CRC Press, Boca Raton, Fla., 2008).
[30] J. E. Olson, Journal of Geophysical Research **98**, 12251 (1993).
[31] R. A. Schultz, International Journal of Rock Mechanics and Mining Sciences **37**, 403 (2000).